NASA Technical Paper 1361

Fluctuating Surface Pressure and Acoustic Radiation for Subsonic Normal Jet Impingement

John S. Preisser

MARCH 1979

NASA

NASA Technical Paper 1361

Fluctuating Surface Pressure and Acoustic Radiation for Subsonic Normal Jet Impingement

John S. Preisser
Langley Research Center
Hampton, Virginia

National Aeronautics
and Space Administration

Scientific and Technical Information Office

1979

SUMMARY

This report presents results from an experimental study of fluctuating surface pressures and far-field noise produced by a subsonic circular jet impinging normally to a large, rigid, flat surface. The tests were performed in an anechoic room for jet Mach numbers from 0.54 to 0.85 and for jet-to-surface heights from 5 to 10 jet diameters. Space and time correlations of surface pressure indicated a radially spreading, decaying pressure field having correlation lengths on the order of one-half the jet diameter with convection speeds between 0.5 and 0.6 of the peak wall-jet velocity. Overall sound pressure level varied as the eighth power of the jet velocity, with noise levels increasing in most directions as the jet was lowered closer to the surface. Large-scale orderly structures in the flow were suggested by the noise spectra which peaked at a Strouhal number of about 0.3.

In addition, an analytical formulation based on Curle's equation and a variation of Powell's image argument for infinite surfaces was given to approximate the apparent noise-producing regions of the flow in terms of cross-correlations and cross-spectra between the surface and far-field measurements. Results pointed to the impingement region of the flow field as the major contributor to the far-field impingement noise.

INTRODUCTION

The impingement of a jet of air or exhaust gas on a surface occurs in many different aerospace vehicles having diverse applications. Short take-off and landing aircraft (STOL), both the externally blown flap and upper surface blowing types, employ a wing-flap surface to deflect jet engine exhaust and provide propulsive lift. Rockets on launch pads often employ thrust deflectors to divert the hot engine exhaust away from the rocket. Thrust reversers are used by jet aircraft after landing to change the direction of thrust in order to bring the aircraft to a quick stop. Although the applications are different, all of these examples involve a jet impinging on a surface. In the process, high levels of fluctuating surface pressure are generated, and intense noise usually results. These high levels are, of course, potentially undesirable situations from the viewpoint of both acoustic fatigue to the structure and acceptable noise standards for the community.

This report presents results from an experimental study of fluctuating surface pressure and acoustic radiation for a subsonic jet impinging normally to a large, flat, rigid

surface. The prime objective was to quantify surface pressure and noise level simultaneously for this simple test arrangement and to establish the interrelation between the two in order to determine the major noise-producing regions of the flow. Jet impingement has been studied extensively in the past. (See, for example, refs. 1 to 18.) Most of the work (e.g., refs. 1 to 10) has been aimed at characterizing the mean flow structure with the goal of identifying and analytically modeling the regions of physically similar flow behavior. Several of the studies (e.g., refs. 5, 11, and 12) have included measurements of the turbulent flow structure. Others (refs. 13 to 15) have devoted a major part of their studies to surface pressure fluctuations resulting from the impingement process. In addition, there exist a few published reports (refs. 16 to 18) that study the noise field produced by jet impingement on very large surfaces. (In contrast there are many noise studies for situations where surface edges play a dominant role.) There are few, if any, published reports which experimentally study either the turbulent flow structure or fluctuating surface pressure simultaneously with the noise field for a very large (infinite) surface. There are several fundamental theoretical studies, such as reference 19, which treat flow over infinite surfaces in general. An attempt to computationally relate the fluid flow and its time-varying properties to the noise field for jet impingement has been made by Woolley, Karamcheti, and Guenther (ref. 20). Pan (ref. 21) has proposed a method for separating surface and volume contributions to the noise field for various flow-surface interaction problems, including jet impingement.

This report presents results based on measurements of far-field noise and fluctuating surface pressure. Overall pressure levels and power spectral densities are given for both measurements. Cross-correlations are presented between pairs of surface measurements and between surface and far-field measurements. In addition, the appendix presents an analytical formulation which approximates the apparent noise-producing regions near the surface in terms of cross-correlations and cross-spectra between surface and far-field measurements. The formulation is based on Curle's equation (ref. 22) and a variation of Powell's image argument for infinite surfaces (ref. 19).

SYMBOLS

A	surface area
a,b	arbitrary stationary random processes
c	speed of sound in fluid medium at rest
d	jet diameter

f	frequency
G_a	measured power spectral density function, $2S_{aa}(f) \quad (0 \leqq f < \infty)$
h	jet height above surface
k	wave number, ω/c
M_j	jet Mach number
p	far-field acoustic pressure
p_s	fluctuating surface pressure
q_j	jet dynamic pressure
$R_{ab}(\tau)$	correlation function, $\langle a(t)\, b(t+\tau) \rangle$
r	distance between far-field observation point and source point, $\lvert \vec{x} - \vec{y} \rvert$
$S_{ab}(\omega)$	power spectral density function, $\int_{-\infty}^{\infty} R_{ab}(\tau)\, e^{-i\omega\tau}\, d\tau$; also $\lvert S_{ab}(\omega) \rvert\, e^{i\phi}$
T_{ij}	Lighthill stress tensor
t	observer time
U	velocity of fluid
U_c	eddy convection velocity
U_j	centerline velocity in jet exit plane
U_m	maximum velocity in wall jet
V	volume region
x	distance to observer position from jet-impingement stagnation point

y	distance to source position from jet-impingement stagnation point
ξ,η	coordinates defining plane normal to surface containing surface microphone positions (refer to fig. 3)
η_m	vertical distance to maximum velocity in wall jet
η_o	vertical height above surface of assumed source
$\eta_{1/2}$	vertical distance to point in wall jet where $U = U_m/2$
θ	angle between surface normal and $\vec{x}$
λ	acoustic wavelength
ξ_{ref}	position of fixed surface microphone used in space-time cross-correlations, 0.44d
ρ	density
$\rho_{ab}(\tau)$	correlation coefficient, $\frac{R_{ab}(\tau)}{\sqrt{R_{aa}(0)\,R_{bb}(0)}}$
τ	delay time
τ_{eddy}	calculated delay time based on eddy convection model, $\frac{r}{c} - \frac{\xi}{\overline{U}_c}$
τ_{meas}	measured delay time
ϕ	phase angle
ψ	angle between $\vec{x}$ and $\vec{y}$
ω	circular frequency, $2\pi f$

Subscripts:

i,j	indices of components of vectors
n	normal to surface

Abbreviations:

dB	decibel, referenced to 20 μPa
OASPL	overall sound pressure level
SPL	sound pressure level

A bar over a symbol indicates root mean square, the brackets $\langle\ \rangle$ denote a time average, an arrow over a symbol indicates a vector, and a prime denotes the image region.

TEST SYSTEM

Facility and Test Apparatus

The tests were performed in an anechoic noise facility at the Langley Research Center. The test chamber of this facility is approximately 7.6 m long, 7.6 m wide, and 7.0 m high. The walls, floor, and ceiling are lined with fiberglass wedges, which were designed for a chamber cutoff frequency of approximately 100 Hz. The entire floor area is covered with removable metal grating.

A photograph of the experimental apparatus in the anechoic room is shown in figure 1. Air from a regulated high-pressure system was supplied continuously into a 0.30-m-diameter flexible hose, through an adapter, and then into a 6.35-cm-diameter pipe. The pipe was bent 90° with a 2.0-m run length to the exit. The last 0.5-m section was machined aluminum pipe, which formed the nozzle. The supporting mechanism for the hose and pipe allowed for adjustments to the position of the pipe over a test surface for the jet impingement tests. The surface was a 3.0-m by 1.8-m by 2.54-cm sheet of polished aluminum alloy. It was made large to minimize the added complications of noise due to edge effects and was rigid and smooth to eliminate any effects of structural vibration or other secondary noise sources. It was fastened about its perimeter to a 12.7-cm steel channel. Rubber was used between the surface and the channel to minimize vibration transmission. The entire surface was supported by a steel frame which placed

the surface about 0.76 m above the floor. For the free-jet tests, the surface, support frame, and the metal grating floor were removed.

Instrumentation and Procedure

One-eighth-inch condenser microphones were used to measure fluctuating surface pressures. The surface was drilled through at 12 positions (radially from the jet-impingement stagnation point) to provide room for the microphones. The microphones were used without their protective grids so that the microphone diaphragms were exposed. The diaphragms were flush with the surface. The microphones and their adapters were isolated from the surface by means of nylon bushings. Details of this arrangement are shown in figure 2. Positions of the surface microphones are given in table I.

A single, 1/2-in. condenser microphone was used to measure the far-field noise. The microphone was placed on a remotely operated boom (shown on the far left-hand side of fig. 1) and was rotated through an arc in a plane perpendicular to the surface. The arc had a radius of 3.05 m and was centered at the stagnation point on the surface.

Data from both the surface microphones and the far-field microphone were FM-recorded on a 14-channel tape recorder at 150 cm/sec. Prior to testing, microphones were selected with similar phase characteristics and the tape recorder channels were chosen to minimize interchannel phase differences. Pretest broad-band calibrations showed that all system interchannel time delays were less than 15 μsec. The frequency response curve for the system was generally flat within ± 1 dB over the recorded frequency range from 200 Hz to 15 000 Hz. The recorded data were reduced by employing a general time-series-analysis computer program to yield overall signal levels, narrow-band power spectra (60-Hz analysis bandwidth), autocorrelations, and cross-correlations. Assuming normality of data and standard statistical methods, it is 90 percent certain that the spectra are within ± 1.1 dB of the true spectra.

Tests were performed at Mach numbers (based on jet centerline velocities) of 0.54, 0.62, 0.70, and 0.85. Ratios of jet height to nozzle diameter were 5, 7, and 10; in addition, the free jet was also tested.

RESULTS AND DISCUSSION

This section presents results from fluctuating-surface-pressure measurements, far-field-noise measurements, and the interrelational properties of the two. It will be helpful, however, to briefly review some previous work and the terminology defined therein. Based on results of reference 1, the jet-impingement flow field can best be described by considering three separate regimes (see fig. 3): (1) the free-jet regime which is upstream of any strong flow-surface interaction effects and where the jet behaves

about the same as it would if no surface were present, (2) the impingement regime where the back pressure caused by the surface strongly alters the free-jet behavior and considerable change in the flow occurs, and (3) the wall-jet regime where the flow is spreading radially outward along the surface and nearly self-similar mean velocity profiles develop in the flow. A sketch of the flow field and definition of the coordinate system used in this report are also presented in figure 3. In general, the extent of the different flow regimes may be functions of jet Mach number and jet height-to-diameter ratio.

Mean Flow Measurements

In this section of the report, typical velocity profiles for the free jet and the wall jet are presented. The measurements were made during an earlier test and are reported in reference 18. Typical radial velocity distributions at several positions downstream are presented for the free jet in figure 4. The data are for a jet exit Mach number of 0.93. Note that the distribution is nonuniform in the jet exit plane as a result of a relatively thick turbulent boundary layer built up within the pipe. However, there is a section of flow symmetric about the centerline of the jet where the velocity is uniform and this centerline level persists for at least 4 jet diameters downstream.

Figure 5 presents normalized velocity distributions in the wall-jet regime of flow, where U_m is the peak velocity in the wall jet and $\eta_{1/2}$ is the vertical height corresponding to $U = U_m/2$. The wall jet, which was first studied by Glauert (ref. 23), is characterized by a thin boundary layer near the surface and a free shear layer above. Glauert found that flow similarity could be achieved if the Reynolds number did not vary appreciably. It is seen in the figure that, for $\xi/d \geq 3$, similarity is reached in agreement with Glauert's analysis.

The impingement regime, which is much more complicated, was not studied in detail in reference 18. However, other studies (refs. 2, 12, and 24) indicate that the regime is dominated by large-scale, well-defined vortex structures in the flow which form at the nozzle exit, propagate downstream, and become strongly altered upon impact with the surface. The impingement regime can be considered contained within the cylindrical region $\eta/d < 2$ and $\xi/d < 3$.

Surface Pressure Measurements

Root-mean-square levels.- Figure 6 presents the fluctuating-surface-pressure coefficient as a function of radial distance measured outward from the jet-impingement stagnation point. The coefficient is expressed as $\bar{p}_s/q_j$, where $\bar{p}_s$ is the root-mean-square fluctuating surface pressure and q_j is the centerline dynamic pressure in the jet exit plane. The results are shown for the four test Mach numbers at a jet height of

5 diameters above the surface. The coefficients are relatively high compared with boundary-layer pressure fluctuations for which coefficients in the neighborhood of 0.006 are typical (ref. 25). Note that although the jet-exit mean flow is compressible, the fluctuating-pressure-coefficient distribution is nearly independent of Mach number. At $\xi/d = 0$, the level is slightly lower than at the two adjacent positions, which would be an indication of the uniform flow along the jet centerline, as shown in figure 4. According to Glauert (ref. 23), for large Reynolds number, the maximum velocity in the wall jet U_m is inversely proportional to the distance from the stagnation point ξ. In this study, in the region $\xi/d > 3$, the fluctuating-pressure coefficient varies as ξ^{-2}. Thus, the fluctuating pressure is directly proportional to the square of the maximum velocity in the wall jet.

Radial distributions of fluctuating-surface-pressure coefficient are presented in figure 7 for the three test jet heights at a fixed jet Mach number of 0.70. Here, the data show a dependence on jet height when $\xi/d < 3$. In the region $0.70 < \xi/d < 3$, the closer the jet to the surface, the higher the fluctuating-pressure level. This is not surprising, since the magnitude of turbulence fluctuations at equivalent stations in the free jet exhibits a similar trend. For $\xi/d > 3$ however, the levels are independent of height. This is consistent with the description of the wall-jet regime. The fluctuating properties in the flow become so dominated by the surface (or wall) that they are not affected by upstream conditions.

Spectra.- The effects on the pressure spectra of the radial surface position, Mach number, and jet height-to-diameter ratio are shown in figures 8, 9, and 10, respectively. Power spectral density of fluctuating surface pressure is presented in figure 8 for various surface microphone positions. The data are for $M_j = 0.70$ and $h/d = 5$. Spectral shapes are strongly dependent on position. Positions from $\xi/d = 0$ to 0.44 are all within direct impingement of the jet and show high levels at all frequencies. Positions from $\xi/d = 1.00$ to 1.80 are in the outer impingement regime and have similar shapes and levels with spectra peaking in the 1000- to 2000-Hz mid-frequency range. Positions from $\xi/d = 3.00$ to 5.20 are all in the wall-jet regime and show a systematic decrease in the high-frequency end of the spectra.

The effect of changes in Mach number on the power spectral density is presented in figure 9 for the stagnation point ($\xi/d = 0$) and for a position in the outer impingement regime ($\xi/d = 1.80$). Spectral shapes are similar for the Mach number range shown. (Data are not shown for $M_j = 0.85$, since these particular surface transducers were damaged during this particular test.)

The effect of changes in jet height is shown in figure 10 for the same two surface positions as in figure 9. Here, the spectral shape varies with h/d. At the stagnation

point (fig. 10(a)) and as h/d is reduced from 10 to 5, the low-frequency power decreases about an order of magnitude. In contrast, in the outer impingement regime (fig. 10(b)), there is only a slight decrease in low-frequency power while the mid- and high-frequency levels increase.

The systematic trend of spectral shapes in the wall-jet regime as evidenced by figure 8, along with the near similarity in wall-jet velocity profiles as derived by Glauert and shown in figure 5, suggested that similarity in the power spectral density of fluctuating surface pressure could perhaps be achieved for the wall-jet regime. Indeed, Hodgson (ref. 13) has shown that similarity does exist for a radial wall jet at low subsonic Mach numbers. A nondimensional power spectral density is plotted in figure 11 as a function of nondimensional frequency. Hodgson nondimensionalized his data with the peak velocity in the wall jet U_m, the vertical distance to the peak velocity η_m, and the distance to that point in the free shear layer $\eta_{1/2}$ where the velocity was $U_m/2$. These values of U and η, obtained from results of reference 18, were also used to nondimensionalize the spectra in figure 11. Data are presented for positions in the wall-jet regime ξ/d from 3.00 to 5.20, jet heights h/d from 5 to 10, and Mach numbers M_j from 0.54 to 0.85. There appears to be a reasonable collapse of the measured results considering the range of data considered. Perhaps more surprising is that these data agree very well on a quantitative basis with Hodgson's data (ref. 13). Hodgson's measurements covered a similar ξ/d range, but h/d was fixed at 0.5 (an entire order of magnitude less than h/d for the present tests) and $M_j < 0.3$. These present results, therefore, show that for the wall jet the fluctuating-surface-pressure power spectral density is dependent on the peak velocity in the wall jet U_m and the thickness of the free shear layer $\eta_{1/2} - \eta_m$ and virtually independent of h/d and M_j over a wide range of both these parameters.

Correlations.- Figure 12 presents broad-band space-time cross-correlations for various microphone positions $\left(\text{relative to } \xi/d = 0.44, \text{ hereafter referred to as } \xi_{ref}\right)$ for the case of $M_j = 0.70$ and $h/d = 5$. A correlation peak was not identifiable for $\xi/d = 3.60$, 4.40, or 5.20. This, again would be an indication of the wall-jet regime, since the statistical properties there are not strongly related to those at $\xi/d = 0.44$. Qualitatively, the curves are similar to those reported in reference 14 for normal jet impingement at a jet velocity of 41 m/sec. It is seen that the statistical properties of fluctuating pressure change along a radial path going outward from the stagnation point. The space-time correlation curves clearly have the character which would be associated with a convected pressure field slowly losing its correlation as convection proceeds. Whereas to an observer fixed in space (a single curve in fig. 12), the pressure is correlated only for a short time, to an observer who moves with the field so as to be always at the position of maximum correlation, the field would appear to lose correlation at a much slower rate. Indeed, an envelope was drawn to the family of curves in figure 12 which defines the

so-called "autocorrelation in the moving frame" (ref. 26). A curve was plotted of separation $\xi - \xi_{ref}$ versus time delay τ for points on the envelope. The result is presented in figure 13(a). The slope was taken at the data points shown and this was interpreted as the local eddy convection speed U_c at these respective points.

Figure 13(b) presents the results for the convection speed, as obtained in this manner. Also, shown for comparison is the value of the peak velocity of flow along the surface obtained from reference 18. Both curves decrease with separation because of radial spreading. The convection speed is less than the peak mean flow velocity, varying between 50 and 60 percent of U_m.

Space cross-correlations of fluctuating surface pressure are presented in figure 14 for several values of h/d at a Mach number of 0.70. The microphone position which corresponded to $\xi/d = 0.44$ was again chosen to be the fixed, reference ξ_{ref} while the other was varied over the remaining outer positions. The correlation curves fall off very rapidly with increasing $\left(\xi - \xi_{ref}\right)/d$, reach a minimum negative value, and then approach zero. As h/d increases, the value of ξ/d corresponding to the first zero crossing increases. This value can be considered to be a measure of the typical eddy size, or correlation length, which is seen to be about one-half of the jet diameter. The correlation curves in figure 14 did not change appreciably with jet Mach number.

It is interesting to note that both the space cross-correlation of figure 14 and the autocorrelation of figure 12 show significant negative values of correlation. Theoretical work by Kraichnan (ref. 27) and later by Hodgson (ref. 13) on particular models of boundary-layer flow indicates that if the fluctuating surface pressure is mainly the result of interaction between the turbulence and mean shear, then the correlation should satisfy the boundary conditions that both the integral length scale

$$\int_{-\infty}^{\infty} R_{p_s p_s}(\xi,0)\, d\xi$$

and the integral time scale

$$\int_{-\infty}^{\infty} R_{p_s p_s}(0,\tau)\, d\tau$$

be almost zero. The present experimental data on the developing wall jet have roughly equivalent positive and negative contributions to the integral of the correlations and hence are consistent with these predictions.

Far-Field Noise Measurements

Overall sound pressure levels.- Figure 15 presents the variation of overall sound pressure level (OASPL) with jet velocity. Results are shown for jet height-to-diameter ratios of 10, 7, and 5 and for the free jet. The data were taken in the far field at a radial distance of 48 jet diameters and at an angle of 55° from the normal. The variation for the free jet follows a U_j^8 law, as expected. The impingement cases also exhibit about the same (or slightly greater) variation. This result is consistent with that found in reference 16 for sound power levels resulting from jet impingement on a large piece of plywood. Note also that for all velocities, the noise level increases as the jet is lowered closer to the surface. Jet impingement increases the noise by more than 6 dB for all cases; hence, one would expect that jet noise reflection, although surely present, is not the only phenomenon involved.

Figure 16 presents the directivity patterns for $M_j = 0.70$ for the various impingement cases and for the free jet. Because of symmetry about a direction normal to the surface, far-field measurements were taken in only one plane and in one quadrant of that plane (see fig. 1). The size of the experimental apparatus prohibited measurements from being taken in the region on the other side of the surface. However, noise levels were anticipated to be extremely low there because of shielding of most of the spectra (except, perhaps for the lowest frequencies) by the surface. The directivity patterns exhibit a general trend of increasing noise with decreasing jet height; however, for $\theta > 50^{\circ}$, the amount of increase is very angle dependent. In the region upstream of the jet, the impingement noise level shows a large increase over that of a free jet, but the increase is not dependent on jet height. Near $\theta = 60^{\circ}$, the h/d dependence is strongest, and large increases in impingement noise are still present. At $\theta = 90^{\circ}$, the h/d dependence becomes insignificant and, in addition, there is little evidence of any noise associated with impingement.

In this regard, it is interesting to note that any noise radiation emanating from the impingement and wall-jet regimes would undergo refraction by the mean flow on its way to the far field. The effect of the velocity profile in the free shear layer would be to refract the acoustic radiation away from the flow direction (the 90° direction). This may account for the observed dropoff in level in figure 16, since the noise in the $\theta = 90^{\circ}$ direction would have originated from sources in the much weaker free-jet regime.

Spectra.- Power spectral density of the far-field noise at several angle positions is presented in figure 17. The spectra are similar over much of the θ range, except for the largest angle which shows much less mid- and high-frequency power. Since refraction is expected to increase with increasing frequency, this result supports the explanation for the dropoff in level near $\theta = 90^{\circ}$ in figure 16. The data shown here are

for one test Mach number and one particular h/d. Other test conditions also revealed a similar θ independence.

Figure 18 presents power spectral density of the far-field noise for several jet Mach numbers. The individual curves show the same systematic increase with Mach number as did the fluctuating surface pressure (refer to fig. 9). A prominent feature of figure 18 is the large amount of energy concentrated in a narrow band around a frequency of 2000 Hz for $M_j = 0.85$. At high flow speeds, the time for large-scale ordered flow patterns leaving the jet to convect to the plate is on the order of the time for acoustic waves resulting from impingement to propagate upstream to the jet exit. Under proper conditions, a feedback loop is formed whereby each successive cycle of the large-scale structure in the jet is triggered by the upstream-traveling pressure waves of the previous cycle. The additional acoustic energy resulting from this is concentrated in a narrow band near the feedback frequency. This phenomenon was first studied by Wagner (ref. 28). Wagner derived the semiempirical relation

$$f = 0.6 \frac{c}{d}\left(\frac{M_j}{3.75M_j - 1.65}\right)$$

to predict the discrete tone frequency. Although Wagner's jets were small (1.5 cm diameter or less), his equation predicts a frequency of about 1800 Hz which is not far below that measured for the much larger jet of the present test. The effects of the narrow-band acoustic energy on the enhancement of the existing broad-band noise are unknown.

The effect of h/d on power spectral density of the far-field noise is presented in figure 19. As with the fluctuating surface pressure in figure 10, the shape is dependent on h/d. Whereas the mid- and high-frequency portions of the spectra show a definite increase in level as the jet is lowered to the surface, the low-frequency end shows an opposite effect. In fact for $h/d = 5$, the low-frequency power approaches that of the free jet. The jet-impingement process, therefore, enhances the noise-producing sources of the free jet to various degrees depending on the frequency range.

The redistribution of acoustic energy as a function of frequency which occurs when a free jet impinges on a surface is made further evident in figure 20. In this figure, one-third-octave band spectra are plotted in nondimensionalized form as a function of Strouhal number. The spectra were taken at $\theta = 55^{\circ}$ and $M_j = 0.70$. The impingement data are for $h/d = 5$. Jet impingement produces a much more peaked spectrum than the free jet, with less energy in the low-frequency bands and more in the mid-frequency range. This mid-frequency range is the same as that which has been reported for the rate of formation of large-scale ordered structures observed in free jets (refs. 29 and 30). Further, it has

been reported (ref. 30) that these structures govern the production of turbulent fluctuations which radiate broad-band jet noise. The present data suggest that this noise-producing process may be enhanced by jet impingement.

Surface Interaction Noise

In the previous two sections of this report, results were presented for the fluctuating surface pressure and the far-field noise. Certain similarities exist between the two sets of results. Both show increasing levels with increasing Mach number and decreasing jet height. Both show increases in the relative amount of low-frequency power as the jet is raised. In addition, both sets of spectra peak in the mid-frequency range (around 1000 Hz). The peak implies that an ordered structure of relatively large scale plays a role in both the surface pressure and acoustic results. Indeed, recent studies of jet noise (for example, ref. 29) indicate large-scale vortex patterns in the free jet being formed at the nozzle exit at an average Strouhal number of about 0.3 based on frequency, jet-exit speed, and jet diameter. This Strouhal number approximately matches the present jet-impingement data peak. Also, in reference 28 it was observed that similar large-scale structures were present in the jet-impingement process and, furthermore, that these structures were responsible for the strong feedback loop and resulting narrow-band acoustic radiation which developed at high Mach numbers (as witnessed by the $M_j = 0.85$ data shown in fig. 18). Hence, there is evidence that large-scale ordered structures are important in the jet-impingement process. The present experimental results, although not providing any new insight into the process of sound production by these structures, do add additional evidence suggesting their importance. Nevertheless, causal relationships between the surface pressure and the noise can be developed and major noise-producing regions of the flow can be identified.

An analysis of surface interaction noise is presented in the appendix. The analysis is based on Curle's equation (ref. 22) and employs a variation of Powell's image argument (ref. 19) for flow over infinite surfaces. A sketch of the real and an image flow system for the jet-impingement process is shown in figure 21. Typical source $\vec{y}$ and field point locations $\vec{x}$ are shown. Powell replaced the surface with the image system and described the far-field noise in terms of both the real and image flow. In the appendix, it is shown that under certain conditions, the impingement noise can also be approximately described by the surface pressures alone. In particular, it is shown that in the geometric and acoustic far fields $\left(|\vec{x}| >> |\vec{y}| \text{ and } |r| >> \lambda\right)$ and when the major acoustic sources are near the surface $\left(k\eta_o << 1\right)$, the autocorrelation of the far-field noise can be approximately expressed as

$$R_{pp}(\vec{x},\tau) \approx -\frac{\cos\theta}{2\pi c x}\int_A \frac{\partial}{\partial\tau} R_{p_s p}(\vec{y},\vec{x},\tau+r/c)\, dA(\vec{y}) \qquad (1)$$

and the auto-power-spectral-density is

$$S_{pp}(\vec{x},\omega) \approx -\frac{i\omega \cos\theta}{2\pi c x} \int_A e^{i\omega r/c} S_{p_s p}(\vec{y},\vec{x},\omega)\, dA(\vec{y}) \tag{2}$$

For the present jet-impingement tests, the assumptions of being in the geometric and acoustic far fields are reasonable. The additional noise sources due to impingement must be contained in the impingement and wall-jet regimes, and not in the free-jet regime. Moreover, the rapid falloff in fluctuating pressure level with radial distance from the stagnation point suggests that the sources are not far from the stagnation point. Hence, $|\vec{x}| >> |\vec{y}|$ and the geometric far-field assumption is most likely met. Also, the power spectral density of the far-field noise is almost entirely contained within the frequency range of from 200 to 10 000 Hz. This would satisfy the acoustic far-field assumption $\left(|\vec{r}| >> \lambda\right)$ over most of this range.

Whether or not equations (1) and (2) are good approximations to the present results depends on the location of the acoustic sources. The actual locations are unknown. For an assumed source at $\xi/d = 3$ and $\eta_o = \eta_{1/2}$, $k\eta << 1$ implies $f << 4000$ Hz. For sources closer to the surface, the frequency limitation would be relaxed. Hence, this assumption is also not unreasonable.

The mean-square acoustic pressure in the far field can be found by setting $\tau = 0$ in equation (1). Then, the contribution to the far-field noise per unit surface area is proportional to the slope of the cross-correlation between surface pressure and far-field acoustic pressure at that value of retarded time, $\tau = r/c$.

Figure 22 presents the normalized cross-correlation function, or the correlation coefficient $\rho_{p_s p}$ as a function of time delay τ for $h/d = 5$ (fig. 22(a)) and $h/d = 10$ (fig. 22(b)). The data are shown for several surface microphone positions within the impingement regime correlated with the far-field position at $\theta = 55^o$. Identifiable correlations were not obtained in the wall-jet regime. For $h/d = 5$, the shape of the three correlations obtained from transducers nearest the stagnation point changes very rapidly, reflecting the closeness of the jet to the surface and the rapidly changing flow in this direct-impingement regime; thereafter the shape varies little and is characterized by a negative peak followed by a positive peak with the level decreasing and the width spreading with increasing ξ/d. For $h/d = 10$, the shape of the first three correlations changes slightly, but the remaining are similar in shape to those of figure 22(a). Siddon (ref. 31) has analytically derived this latter shape for the cross-correlation by assuming a hydrodynamic pressure field with properties of convection and decay. These properties were present in the current tests, as was shown in a previous section of this report. According

to Siddon, who assumed "direct" radiation from the surface to the far field, the far-field noise is proportional to the slope of the cross-correlation at $\tau = r/c$. His analytic model placed this particular delay time at the point between the negative and positive peaks where the correlation crosses the τ-axis.

To find the contribution of each surface position to the far-field noise requires taking the slope of the correlation function at $\tau = r/c$. These particular delay times are identified by upward-pointing arrows in figure 22. It is seen that as ξ/d increases, the correlations occur at an earlier time than the arrow indicates. The actual slope at $\tau = r/c$ would then be a small number compared with the slope at an earlier time (between the negative and positive peaks) where the rate of change of the function is largest. (This earlier time is indicated by the downward-pointing arrow.) This difference in times suggests that these outer surface positions do not radiate directly to the far field.

The data of figure 22 are replotted in figure 23 to better compare the direct acoustic travel time ($\tau = r/c$) with the earlier time corresponding to the maximum slope of the correlation function $\left(\tau_{meas}\right)$. Slopes were not calculated for the first three correlations because of the uncertainty in which slope to choose. As expected from the previous figure, for the remaining correlations, the direct acoustic travel time shows large differences from the maximum slope as ξ/d increases. Also shown in the figure are calculated delay times based on an eddy convection model $\left(\tau_{eddy}\right)$. That is, assume that the most intense noise is created upon impact of the jet with the wall (in the region, $\xi/d < 1$). The time for radiation to the far field should be very near r/c. Subsequently, the noise-producing eddies convect radially outward. Between any two surface positions, the average convection speed $\overline{U}_c$ can be obtained from the fluctuating-surface-pressure cross-correlation. For each position ξ/d, a delay time τ_{eddy} equal to $r/c - \xi/\overline{U}_c$ was calculated. The calculated results agree well with the measured results. Hence, it appears that the most intense noise radiates from the impingement regime. The smaller values of delay time for $h/d = 10$ compared with $h/d = 5$ may be attributed to the lower convection velocities for the former.

Additional information on noise source regions can be obtained by examining the cross-spectrum. Note that, while the far-field autospectrum is a real function, the cross-spectrum is complex. Then the contribution to the far-field noise per unit surface area may be written as

$$\frac{dS_{pp}(\vec{x},\omega)}{dA(\vec{y})} \approx \frac{\omega \cos\theta}{2\pi xc} \sin\left(\frac{\omega r}{c} + \phi\right) \left|S_{p_s p}(\vec{x},\vec{y},\omega)\right| \tag{3}$$

A quantitative evaluation of the noise by integration over the surface would require many more surface pressure measurements to define the cross-spectra for all $\bar{y}$ and is beyond the scope of the present investigation. However, qualitatively it is seen that the noise is proportional to the magnitude of the cross-spectra. The frequency factor, ω, indicates that the far-field noise spectra should rise faster than the cross-spectra at low frequency and fall off slower for high frequencies. The sine factor oscillates very rapidly since $r >> \lambda$ and produces major reinforcements and cancellations from different positions on the surface. This in itself, would make numerical integration a tenuous task. The cosine factor resulted from the choice of focusing on the surface pressures rather than the turbulence itself. Indeed, it was seen in figure 16 that the far-field noise displayed a directivity that dropped off rapidly as θ approached 90^{o}

CONCLUSIONS

Results have been presented from an experimental study of the fluctuating surface pressure and far-field noise produced by a subsonic jet impinging normally to a large, rigid surface. The tests were performed in an anechoic room for jet Mach numbers from 0.54 to 0.85 and for jet-to-surface heights of from 5 to 10 jet diameters. An analytical formulation was given to establish the relationship between surface pressure and far-field noise. It was found that

1. In the geometric and acoustic far fields and for cases where the noise sources are near the surface, apparent localized noise-producing regions of the flow can be found through cross-correlations of fluctuating surface pressure and far-field acoustic pressure. Experimentally determined cross-correlations indicated the inner part of the impingement regime within one jet diameter of the stagnation point to be the major contributor to impingement noise.

2. Far-field noise spectra due to jet impingement were highly peaked at a Strouhal number of 0.3; this result suggests that large-scale, orderly structures in the flow may be involved in the process of sound production.

3. Power spectral density measurements of far-field noise revealed large changes in spectral shape (frequency content and level) with jet height but showed little change in shape with jet Mach number except for $M_j = 0.85$ where a feedback mechanism caused high-amplitude, narrow-band acoustic radiation.

4. Overall sound pressure level varied as the eighth power of the jet velocity, with noise levels increasing in most directions as the jet was lowered closer to the surface.

5. Directivity patterns showed a weak dependence on direction, except for directions nearly parallel to the surface where the level dropped considerably.

6. Space-time correlations of surface pressure indicated a radially spreading, convecting, decaying pressure field with correlation lengths on the order of one-half the jet diameter and convection speeds ranging between 0.5 and 0.6 of the peak wall-jet velocity.

7. Power spectral density measurements of surface pressure in the impingement regime revealed large changes in level and shape with surface location and jet height but showed very little change in shape with jet Mach number (in the range from 0.54 to 0.70). In the wall-jet regime, normalization of the spectral data was achieved over the entire range of test variables by using the peak velocity of the wall jet, the vertical distance to the peak velocity, and the distance to the point in the free shear layer where the velocity was one-half the peak value.

8. Root-mean-square surface pressures were proportional to jet exit dynamic pressure over all Mach numbers, but were not proportional in the impingement region for all jet heights.

Langley Research Center
National Aeronautics and Space Administration
Hampton, VA 23665
December 19, 1978

APPENDIX

ANALYSIS OF SURFACE INTERACTION NOISE

Consider a region of turbulent flow in which a stationary rigid body is present. The acoustic pressure radiated from such a region was given by Curle (ref. 22), as an extension to Lighthill's general theory of aerodynamic sound (ref. 32):

$$p(\vec{x},t) = -\frac{1}{4\pi}\frac{\partial}{\partial x_i}\int_A \frac{P_i(\vec{y},t-r/c)}{r}\,dA(\vec{y}) + \frac{1}{4\pi}\frac{\partial^2}{\partial x_i\,\partial x_j}\int_V \frac{T_{ij}(\vec{y},t-r/c)}{r}\,dV(\vec{y}) \quad \text{(A1)}$$

where $\vec{y}$ locates the source points, $\vec{x}$ is a field point, P_i is the force per unit area exerted on the fluid by the surface in the x_i-direction, T_{ij} is the Lighthill stress tensor, and $r = |\vec{x} - \vec{y}|$. The first term in equation (A1) is equivalent to the sound generated in a medium at rest by a distribution of dipoles of strength P_i. Both shear and normal stress fluctuations may comprise P_i. The second term is the well-known Lighthill integral for turbulence-generated quadrupole noise.

Now consider the application of Curle's equation to a jet impinging on a surface. Assume that surface shear stresses are small compared with the intense normal fluctuating surface pressures measured. A purely passive role is played by surface pressures in the radiation of noise for flow over a rigid, infinite surface. This was demonstrated by Powell (ref. 19) who applied Curle's equation to the real flow system and to an image system (which replaced the real surface, see fig. 21); that is, for the real system, the far-field noise was given by

$$p(\vec{x},t) = -\frac{1}{4\pi}\frac{\partial}{\partial x_n}\int_A \frac{p_s(\vec{y},t-r/c)}{r}\,dA(\vec{y}) + \frac{1}{4\pi}\frac{\partial^2}{\partial x_i\,\partial x_j}\int_V \frac{T_{ij}(\vec{y},t-r/c)}{r}\,dV(\vec{y}) \quad \text{(A2)}$$

where p_s represents the fluctuating surface pressure and x_n is in the direction of the outward normal (also, η-direction). The image system does not contribute noise to the far field; hence,

$$0 = -\frac{1}{4\pi}\frac{\partial}{\partial x_n}\int_{A'} \frac{p'_s(\vec{y},t-r'/c)}{r'}\,dA(\vec{y}) + \frac{1}{4\pi}\frac{\partial^2}{\partial x_i\,\partial x_j}\int_{V'} \frac{T'_{ij}(\vec{y},t-r'/c)}{r'}\,dV(\vec{y}) \quad \text{(A3)}$$

Now the outward normal to surface A' is the negative of the normal to A. Hence, adding both equations as Powell did yields

APPENDIX

$$p(\vec{x},t) = \frac{1}{4\pi}\frac{\partial}{\partial x_i\,\partial x_j}\int_V \frac{T_{ij}(\vec{y},t-r/c)}{r}\,dV(\vec{y}) + \frac{1}{4\pi}\frac{\partial}{\partial x_i\,\partial x_j}\int_{V'} \frac{T'_{ij}(\vec{y},t-r'/c)}{r'}\,dV(\vec{y})$$

$$= \frac{1}{4\pi}\frac{\partial}{\partial x_i\,\partial x_j}\int_{V+V'} \frac{T_{ij}(\vec{y},t-r/c)}{r}\,dV(\vec{y}) \qquad \text{(A4)}$$

(The last expression is a shorthand notation used by Powell.) By comparing this result with equation (A1), it is seen that the volume integral over the image system provides the same contribution to the far-field noise as does the surface integral over the actual surface. Since the image system is purely a reflection of the real system, Powell concluded that the role of the rigid, infinite surface was passive, merely reflecting the sound generated by the flow.

For the present test, this situation would seem to apply very well. The highly polished, large, rigid surface would serve to deflect and turn the flow from the initial direction of the jet, and thereby increase the flow turbulence levels. The turbulence would generate quadrupole noise, in accordance with Lighthill. The far-field microphone would receive this noise both directly and reflected from the surface. Indeed, the experimental acoustic data show a sizable increase in noise level for jet impingement over that of a free jet. Also, the data show a U_j^8 velocity dependence, which is consistent with that obtained by Lighthill for quadrupole-generated jet noise.

To attempt to analyze the far-field radiation in terms of T_{ij}, however, would be a prodigious task beyond the scope of the present endeavor. Instead, it was decided to study the fluctuating surface pressure p_s, which is a much less formidable undertaking. The task remained to relate p_s directly to the far-field acoustic pressure p. This can be accomplished by recasting the image argument of Powell with a different emphasis: Instead of adding equations (A2) and (A3), subtract them. The result is

$$p(\vec{x},t) = -\frac{1}{2\pi}\frac{\partial}{\partial x_n}\int_A \frac{p_s(\vec{y},t-r/c)}{r}\,dA(\vec{y}) + \frac{1}{4\pi}\frac{\partial^2}{\partial x_i\,\partial x_j}\int_{V-V'} \frac{T_{ij}(\vec{y},t-r/c)}{r}\,dV(\vec{y}) \qquad \text{(A5)}$$

(The shorthand notation $\int_{V-V'}$ is used to indicate that the image system is subtracted from the real flow system.) This form of the equation for the far-field noise emphasizes the surface term (the doubling of the integral includes the effect of reflection) at the expense of the volume terms.

It will be useful to the discussion on surface interaction noise to establish how the surface-to-far-field cross-correlations and cross-spectra relate to the far-field noise.

APPENDIX

By performing the spatial differentiation on the integrals in equation (A5) and considering the geometric and acoustic far fields, where $|\vec{x}| >> |\vec{y}|$ and $r >> \lambda$, the far-field acoustic pressure becomes

$$p(\vec{x},t) = \frac{\cos\theta}{2\pi cx}\int_A \frac{\partial}{\partial t} p_s(\vec{y},t-r/c)\, dA(\vec{y}) + \frac{x_i x_j}{4\pi c^2 x^3}\int_{V-V'} \frac{\partial^2}{\partial t^2} T_{ij}(\vec{y},t-r/c)\, dV(\vec{y}) \qquad (A6)$$

where θ is the angle between the outward normal and the field point $\vec{x}$.

If equation (A6) is multiplied with the complex conjugate of the acoustic pressure, $p^*(x,\hat{t})$ at a new time $\hat{t}$ and then a time average is taken, the result is

$$\left\langle p(\vec{x},t)\, p^*(\vec{x},\hat{t})\right\rangle = \frac{\cos\theta}{2\pi cx}\int_A \left\langle \frac{\partial}{\partial t} p_s(\vec{y},t-r/c)\, p^*(\vec{x},\hat{t})\right\rangle dA(\vec{y})$$

$$+ \frac{x_i x_j}{4\pi c^2 x^3}\int_{V-V'} \left\langle \frac{\partial^2}{\partial t^2} T_{ij}(\vec{y},t-r/c)\, p^*(\vec{x},\hat{t})\right\rangle dV(\vec{y}) \qquad (A7)$$

If p, p_s, and T_{ij} represent stationary random variables and if $\hat{t} = t + \tau$, then

$$R_{pp}(\vec{x},\tau) = -\frac{\cos\theta}{2\pi cx}\int_A \frac{\partial}{\partial \tau} R_{p_s p}(\vec{y},\vec{x},\tau+r/c)\, dA(\vec{y})$$

$$+ \frac{x_i x_j}{4\pi c^2 x^3}\int_{V-V'} \frac{\partial^2}{\partial \tau^2} R_{T_{ij}p}(\vec{y},\vec{x},\tau+r/c)\, dV(\vec{y}) \qquad (A8)$$

where $R(\tau)$ is the autocorrelation or cross-correlation function and forms a Fourier transform pair with the auto- or cross-power-spectral-density, respectively,

$$S(\omega) = \int_{-\infty}^{\infty} R(\tau)\, e^{-i\omega\tau}\, d\tau$$

$$R(\tau) = \frac{1}{2\pi}\int_{-\infty}^{\infty} S(\omega)\, e^{i\omega\tau}\, d\omega$$

Siddon (ref. 31) has previously demonstrated a similar form of Curle's equation and applied it to small circular planform airfoils immersed in low-speed open jet airflow. Siddon neglected the volume integral from the outset in equation (A1), and the result was

that the fraction of acoustic radiation per unit area dR_{pp}/dA from the surface was proportional to the slope of the cross-correlation function $\partial R_{p_s p}/\partial\tau$ at the appropriate value of retarded time. The present result, equation (A8), has an additional term because of the difference between the turbulence-generated noise in the flow and in the image space. Under certain conditions, as will now be shown, this difference becomes small and may be neglected. First change over to the frequency domain, by taking the Fourier transform of both sides of equation (A8)

$$S_{pp}(\vec{x},\omega) = -\frac{\cos\theta}{2\pi cx}\int_{-\infty}^{\infty}\int_{A}\frac{\partial}{\partial\tau}R_{p_s p}(\vec{y},\vec{x},\tau+r/c)\,e^{-i\omega\tau}\,dA(\vec{y})\,d\tau$$

$$+\frac{x_i x_j}{4\pi c^2 x^3}\int_{-\infty}^{\infty}\int_{V-V'}\frac{\partial^2}{\partial\tau^2}R_{T_{ij}p}(\vec{y},\vec{x},\tau+r/c)\,e^{-i\omega\tau}\,dV(\vec{y})\,d\tau \qquad \text{(A9)}$$

Integrating by parts (once on the surface integral and twice on the volume integral) results in

$$S_{pp}(\vec{x},\omega) = -\frac{i\omega\cos\theta}{2\pi cx}\int_{A}\int_{-\infty}^{\infty}R_{p_s p}(\vec{y},\vec{x},\tau+r/c)\,e^{-i\omega\tau}\,d\tau\,dA(\vec{y})$$

$$-\frac{\omega^2 x_i x_j}{4\pi c^2 x^3}\int_{V-V'}\int_{-\infty}^{\infty}R_{T_{ij}p}(\vec{y},\vec{x},\tau+r/c)\,e^{-i\omega\tau}\,d\tau\,dV(\vec{y}) \qquad \text{(A10)}$$

or from the definition of the cross-spectrum,

$$S_{pp}(\vec{x},\omega) = -\frac{i\omega\cos\theta}{2\pi cx}\int_{A}e^{i\omega r/c}\,S_{p_s p}(\vec{y},\vec{x},\omega)\,dA(\vec{y})$$

$$-\frac{\omega^2 x_i x_j}{4\pi c^2 x^3}\int_{V-V'}e^{i\omega r/c}\,S_{T_{ij}p}(\vec{y},\vec{x},\omega)\,dV(\vec{y}) \qquad \text{(A11)}$$

Now, it has previously been assumed that noise measurements were taken in the geometric far field, where $|\vec{x}| >> |\vec{y}|$. Then the contribution of the volume integrals in equation (A11) becomes that due to the actual source distribution together with that due to an image source distribution of opposite sign and equal absolute value located at points inverse with respect to $\eta = 0$ to the points of the actual distribution. The integrand can then be written as

APPENDIX

$$\left(e^{i\omega r/c} - e^{i\omega r'/c}\right) S_{T_{ij}p}$$

In the far field (refer to fig. 21),

$$r = |\vec{x} - \vec{y}| = \left(x^2 + y^2 - 2xy \cos \psi\right)^{1/2} \approx x - y \cos \psi$$

and

$$r' = |\vec{x} - \vec{y}'| \approx x - y \cos \psi + 2\eta_o \cos \theta$$

where η_o is the vertical height of the assumed source at $\vec{y}$ above the surface.

The integrand can then be expressed as

$$\left(e^{ik(x-y \cos \psi)} - e^{ik(x-y \cos \psi+2\eta_o \cos \theta)}\right) S_{T_{ij}p}$$

or

$$-2i \sin\left(k\eta_o \cos \theta\right) e^{ik(x-y \cos \psi+\eta_o \cos \theta)} S_{T_{ij}p}$$

Hence, for $k\eta_o << 1$, the integral vanishes. The effect of sources within an acoustic wavelength of the boundary tends to be canceled by the effect of the image sources.

It should be pointed out that Doak (ref. 33) has theoretically studied acoustic radiation from a turbulent fluid containing surfaces by means of Green functions G. He showed for an infinite plane that either the volume sources and their images or fluctuations of the pressure on the surface could be examined depending on whether for a boundary condition $\partial G/\partial x_n$ or G was chosen to vanish on A. The present formulation, using Curle's equation as the starting point, is equivalent.

In summary, in the geometric and acoustic far fields, and for cases where the sources are near the surface $\left(k\eta_o << 1\right)$, the autocorrelation of the far-field noise can be approximately expressed as (eq. (1))

$$R_{pp}(\vec{x}, \tau) \approx -\frac{\cos \theta}{2\pi c x} \int_A \frac{\partial}{\partial \tau} R_{p_s p}(\vec{y}, \vec{x}, \tau + r/c)\, dA(\vec{y}) \tag{A12}$$

and the auto-power-spectral-density as (eq. (2))

APPENDIX

$$S_{pp}(\bar{x},\omega) \approx -\frac{i\omega \cos\theta}{2\pi c x} \int_A e^{i\omega r/c} S_{p_s p}(\bar{y},\bar{x},\omega)\, dA(\bar{y}) \tag{A13}$$

Hence, measurements of fluctuating surface pressure can be thought of as local indicators of turbulence in the flow and cross-correlations and cross-spectra between surface pressure and far-field acoustic pressure can be thought of as a measure of the strength of apparent localized noise-producing regions of the flow.

REFERENCES

1. Donaldson, Coleman Dup.; and Snedeker, Richard S.: A Study of Free Jet Impingement. Part 1. Mean Properties of Free and Impinging Jets. J. Fluid Mech., vol. 45, pt. 2, Jan. 30, 1971, pp. 281-319.

2. Ludwig, G. R.: An Investigation of the Flow in Uniform and Nonuniform Jets Impinging Normally on a Flat Surface. AIAA Paper No. 64-796, Oct. 1964.

3. Bradbury, L. J. S.: The Impact of an Axisymmetric Jet Onto a Normal Ground. Aeronaut. Q., vol. XXIII, pt. 2, May 1972, pp. 141-147.

4. Brady, W. Gordon; and Ludwig, Gary: Theoretical and Experimental Studies of Impinging Uniform Jets. J. American Helicopter Soc., vol. 8, no. 2, Apr. 1963, pp. 1-13.

5. Witze, Peter Ostrander: A Study of Impinging Axisymmetric Turbulent Flows: The Wall Jet, the Radial Jet, and Opposing Free Jets. Ph. D. Thesis, Univ. of California, [1974].

6. Poreh, Michael; and Cermak, J. E.: Flow Characteristics of a Circular Submerged Jet Impinging Normally on a Smooth Boundary. Proceedings of the Sixth Midwestern Conference on Fluid Mechanics, Univ. of Texas, Sept. 1959, pp. 198-212.

7. Govindan, A. P.; and Raju, K. Subba: Hydrodynamics of a Radial Wall Jet. Trans. ASME, Ser. E: J. Appl. Mech., vol. 41, no. 2, June 1974, pp. 518-519.

8. Hrycak, Peter; Lee, David T.; Gauntner, James W.; and Livingood, John N. B.: Experimental Flow Characteristics of a Single Turbulent Jet Impinging on a Flat Plate. NASA TN D-5690, 1970.

9. Ojha, S. K.; and Gollakota, Satyanarayana: Jet Impingement on a Curved Surface. AIAA J., vol. 15, no. 4, Apr. 1977, pp. 453-454.

10. Poreh, M.; Tsuei, Y. G.; and Cermak, J. E.: Investigation of a Turbulent Radial Wall Jet. Trans ASME, Ser. E: J. Appl. Mech., vol. 34, no. 2, June 1967, pp. 457-463.

11. Donaldson, Coleman Dup.; Snedeker, Richard S.; and Margolis, David P.: A Study of Free Jet Impingement. Part 2. Free Jet Turbulent Structure and Impingement Heat Transfer. J. Fluid Mech., vol. 45, pt. 3, Feb. 15, 1971, pp. 477-512.

12. Foss, J. F.; and Kleis, S. J.· Vorticity and Acoustics Measurements in Vertically Impinging Jet Flows. Third Interagency Symposium on University Research in Transportation Noise, Univ. of Utah, Nov. 1975, pp. 425-443.

13. Hodgson, Thomas H.: Pressure Fluctuations in Shear Flow Turbulence. Ph. D. Thesis, Univ. of London, 1962.

14. Strong, D. R.; Siddon, T. E.; and Chu, W. T.: Pressure Fluctuations on a Flat Plate With Oblique Jet Impingement. NASA CR-839, 1967.

15. Westley, R.; Woolley, J. H.; and Brosseau, P.: Surface Pressure Fluctuations From Jet Impingement on an Inclined Flat Plate. Symposium on Acoustic Fatigue, AGARD-CP-113, May 1973, pp. 4-1 – 4-17.

16. Olsen, William A.; Miles, Jeffrey H.; and Dorsch, Robert G.: Noise Generated by Impingement of a Jet Upon a Large Flat Board. NASA TN D-7075, 1972.

17. McKinzie, Daniel J., Jr.; and Burns, Robert J.: Analysis of Noise Produced by Jet Impingement Near the Trailing Edge of a Flat and a Curved Plate. NASA TM X-3171, 1975.

18. Schloth, Arthur P.: Measurements of Mean Flow and Acoustic Power for a Subsonic Jet Impinging Normal to a Large Rigid Surface. NASA TM X-72803, 1976.

19. Powell, Alan: Aerodynamic Noise and the Plane Boundary. J. Acoust. Soc. America, vol. 32, no. 8, Aug. 1960, pp. 982-990.

20. Woolley, J. P.; Karamcheti, K.; and Guenther, J. L.: An Analytical Study of Noise Generation by Subsonic Flows in the Presence of Rigid Surfaces. NASA CR-145027, 1976.

21. Pan, Y. S.: Cross-Correlation Methods for Studying Near- and Farfield Noise Characteristics of Flow-Surface Interactions. J. Acoust. Soc. America, vol. 58, no. 3, Sept. 1975, pp. 586-594.

22. Curle, N.: The Influence of Solid Boundaries Upon Aerodynamic Sound. Proc. R. Soc. (London), ser. A, vol. 231, no. 1187, Sept. 1955, pp. 505-514.

23. Glauert, M. B.: The Wall Jet. J. Fluid Mech., vol. 1, pt. 6, Dec. 1956, pp. 625-643.

24. Yokobori, Seiichi; Kasagi, Nobuhide; and Hirata, Masaru: Characteristic Behaviour of Turbulence in the Stagnation Region of a Two-Dimensional Submerged Jet Impinging Normally on a Flat Plate. Symposium on Turbulent Shear Flows – Volume I, Pennsylvania State Univ., Apr. 1977, pp. 3.17-3.25.

25. Willmarth, W. W.: Space-Time Correlations and Spectra of Wall Pressure in a Turbulent Boundary Layer. NASA MEMO 3-17-59W, 1959.

26. Ff. Williams, J. E.: On Convected Turbulence and Its Relation to Near Field Pressure, U.S.A.A. Rep. No. 109, Univ. of Southampton, June 1960.

27. Kraichnan, Robert H.: Pressure Fluctuations in Turbulent Flow Over a Flat Plate. J. Acoust. Soc. America, vol. 28, no. 3, May 1956, pp. 378-390.

28. Wagner, F. R.: The Sound and Flow Field of an Axially Symmetric Free Jet Upon Impact on a Wall. NASA TT F-13942, 1971.

29. Crow, S. C.; and Champagne, F. H.: Orderly Structure in Jet Turbulence. J. Fluid Mech., vol. 48, pt. 3, Aug. 16, 1971, pp. 547-591.

30. Moore, C. J.: The Role of Shear-Layer Instability Waves in Jet Exhaust Noise. J. Fluid Mech., vol. 80, pt. 2, Apr. 25, 1977, pp. 321-367.

31. Siddon, Thomas E.: Surface Dipole Strength by Cross-Correlation Method. J. Acoust. Soc. America, vol. 53, no. 2, Feb. 1973, pp. 619-633.

32. Lighthill, M. J.: On Sound Generated Aerodynamically. I. General Theory. Proc. R. Soc. (London), ser. A, vol. 211, no. 1107, Mar. 20, 1952, pp. 564-587.

33. Doak, P. E.: Acoustic Radiation From a Turbulent Fluid Containing Foreign Bodies. Proc. R. Soc. London, ser. A, vol. 254, no. 1276, Jan. 19, 1960, pp. 129-145.

TABLE I.- LOCATION OF SURFACE MICROPHONES

Position	ξ/d
1	0
2	.22
3	.44
4	.70
5	1.00
6	1.40
7	1.80
8	2.40
9	3.00
10	3.60
11	4.40
12	5.20

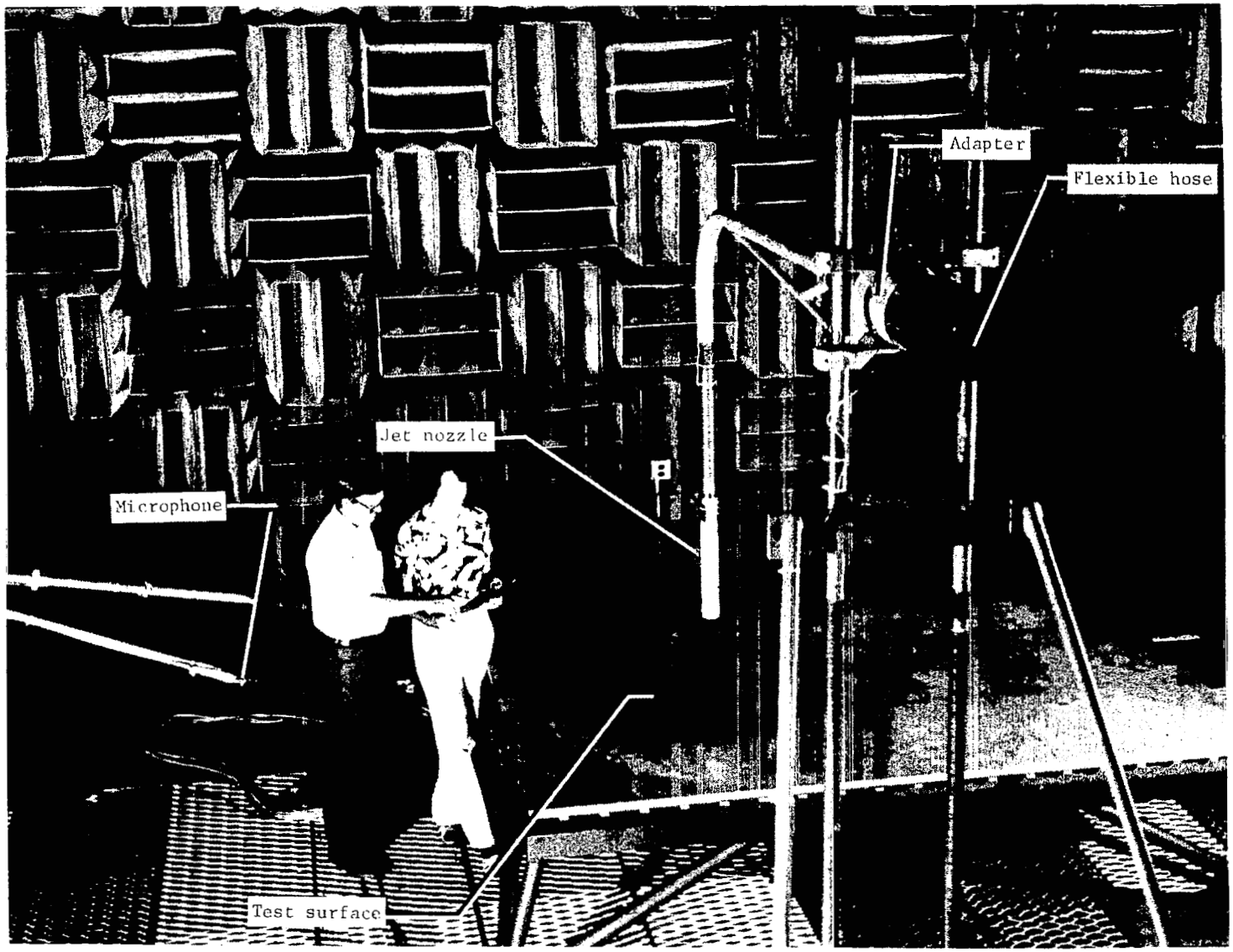

L-75-4478.1

Figure 1.- Experimental apparatus in anechoic room.

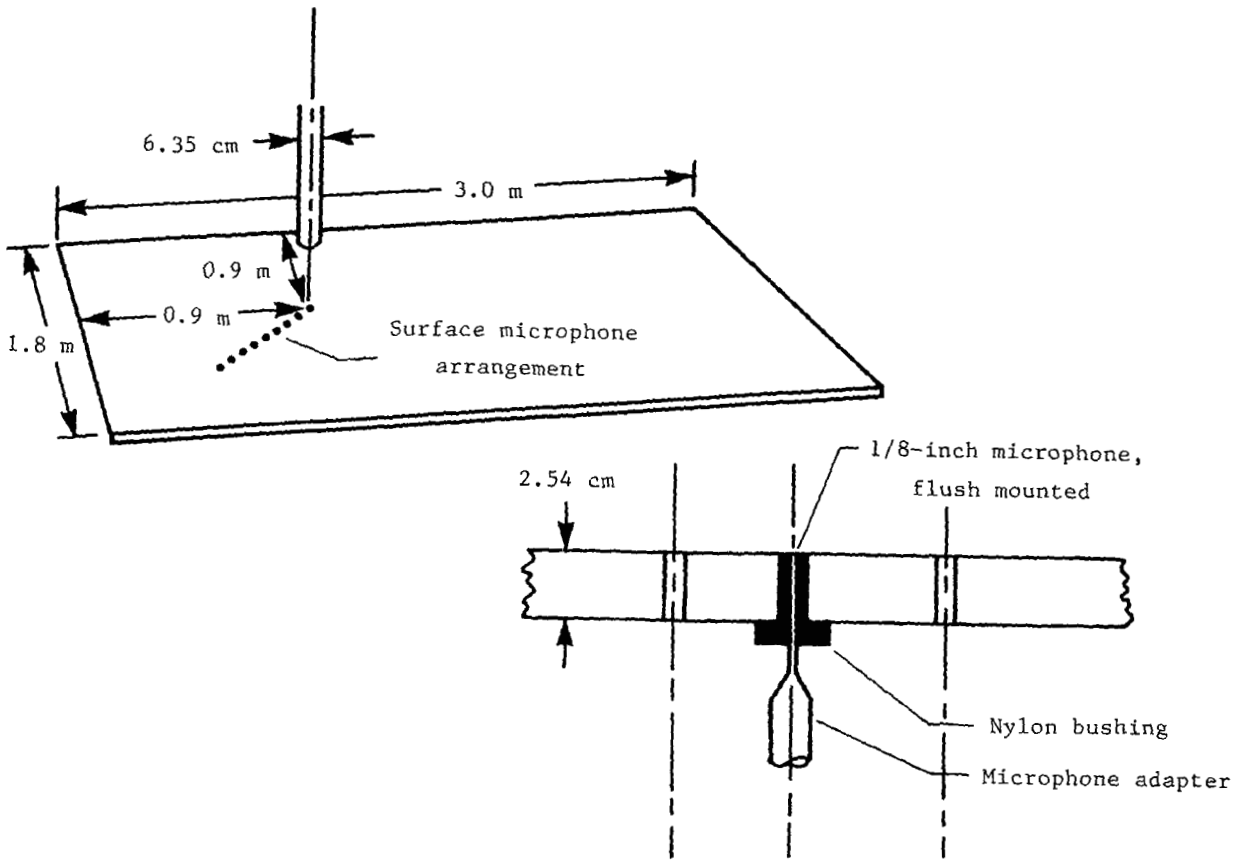

Figure 2.- Surface microphone arrangement and cross-section view showing typical microphone installation.

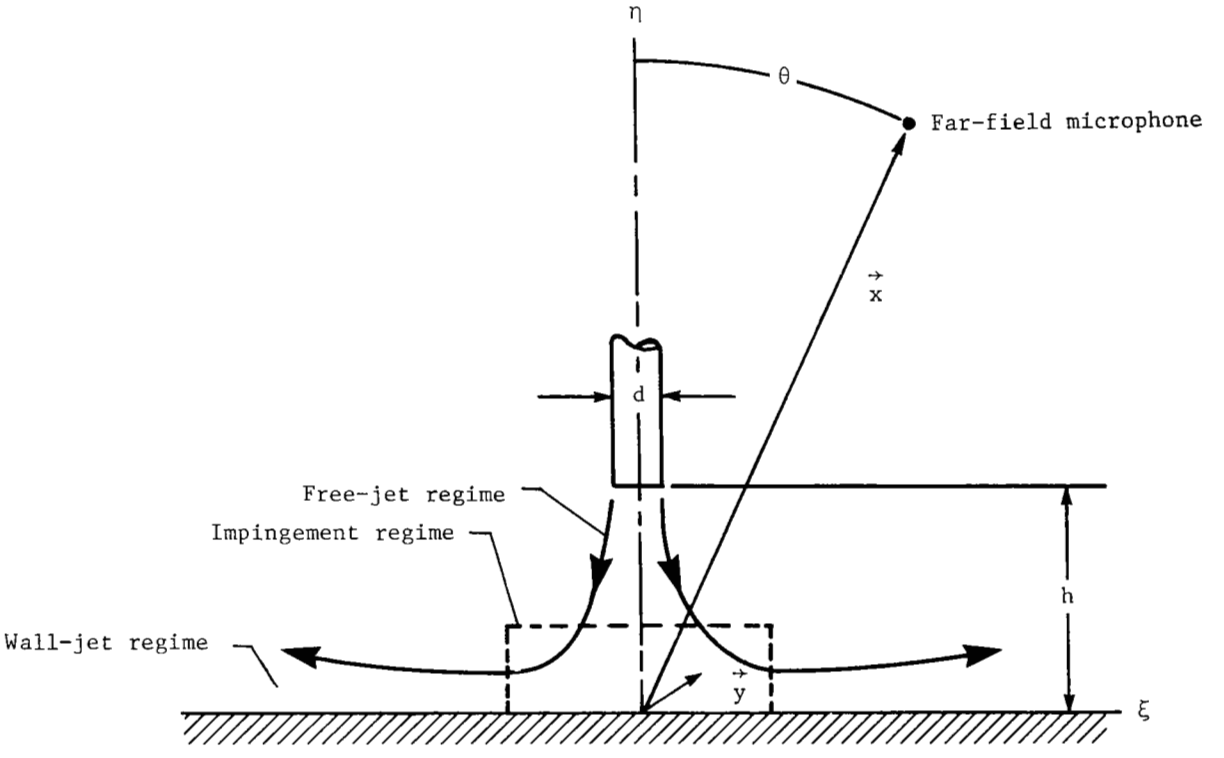

Figure 3.- Sketch showing jet-impingement flow field, flow regimes, and coordinate system.

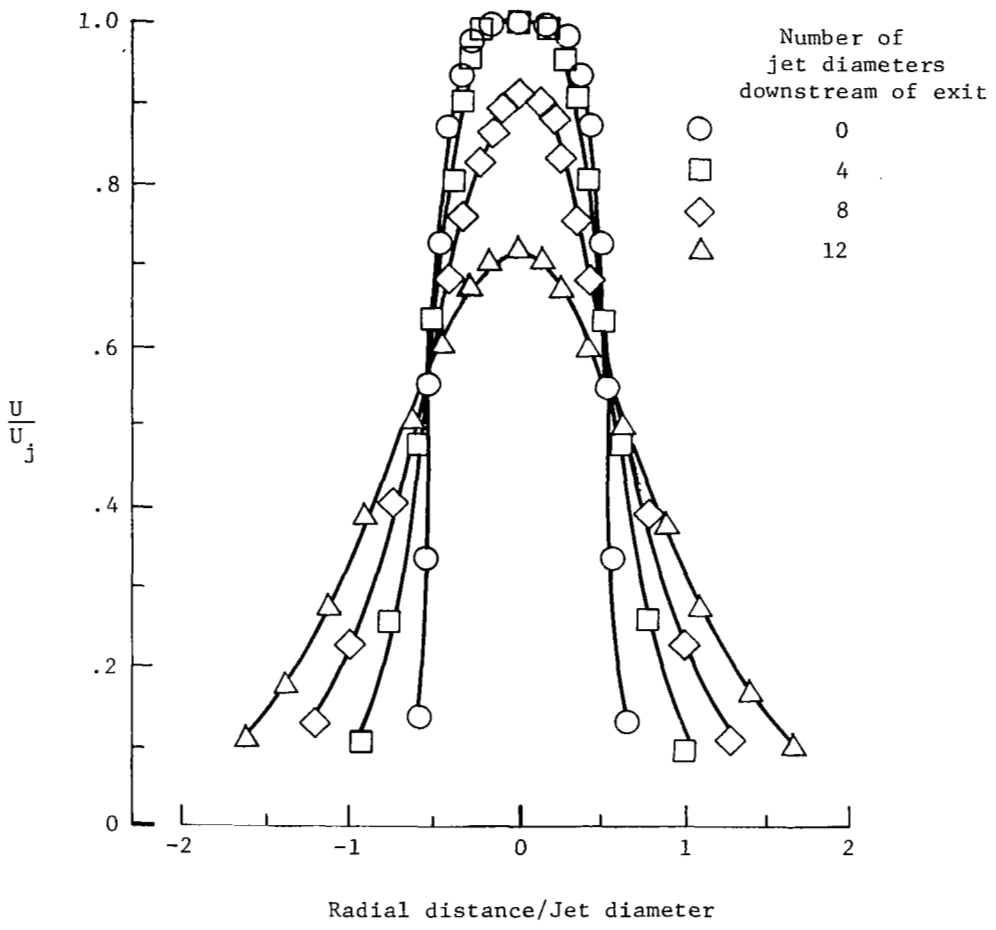

Figure 4.- Typical radial distributions of velocity for free jet. $M_j = 0.93$. (From ref. 18.)

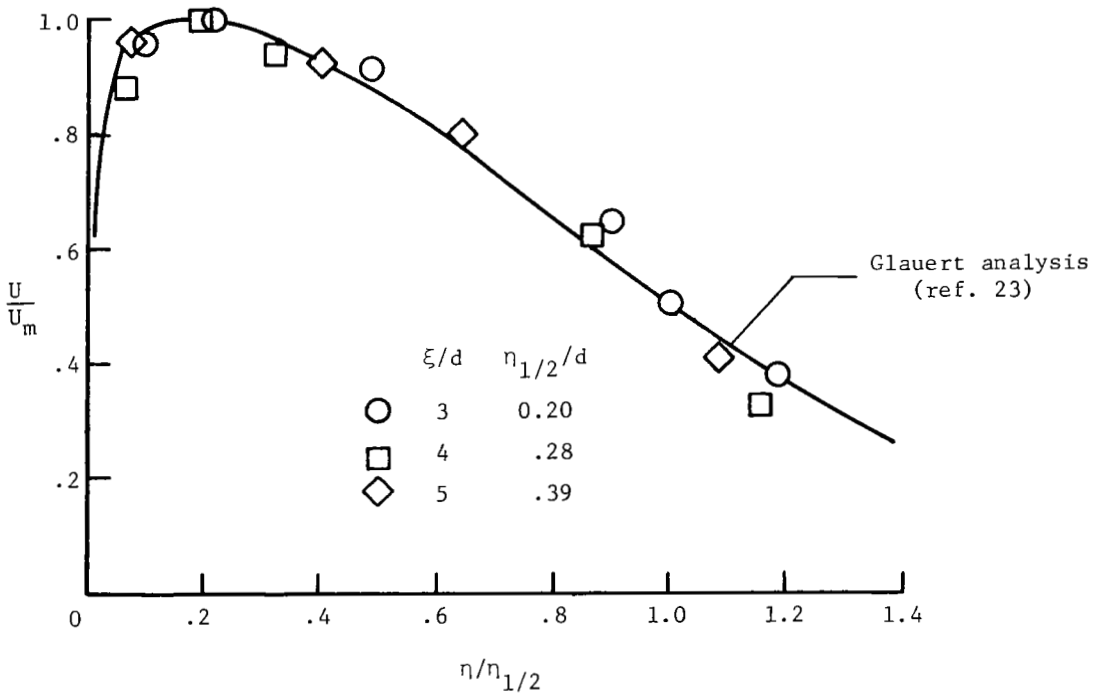

Figure 5.- Normalized velocity distributions in the wall-jet region. $M_j = 0.93$; $h/d = 5$. (From ref. 18.)

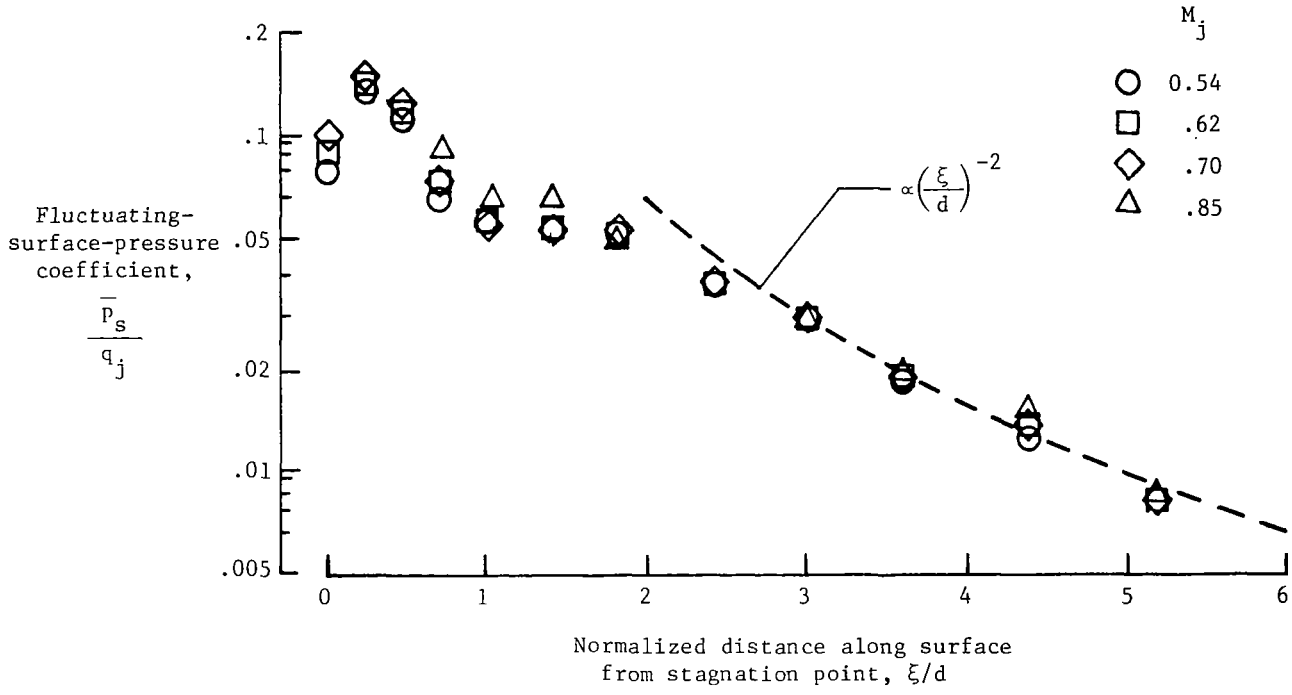

Figure 6.- Radial distribution of fluctuating-surface-pressure coefficient for several jet Mach numbers. h/d = 5.

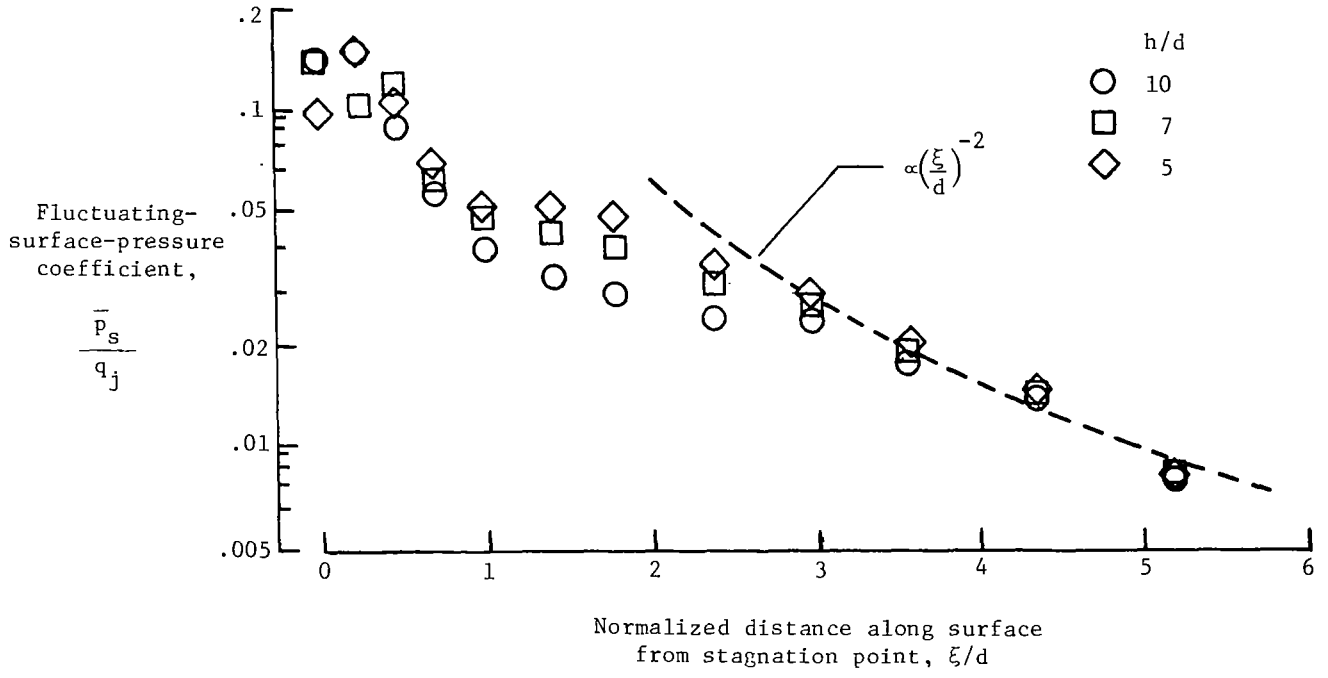

Figure 7.- Radial distribution of fluctuating-surface-pressure coefficient for several jet heights. $M_j = 0.70$.

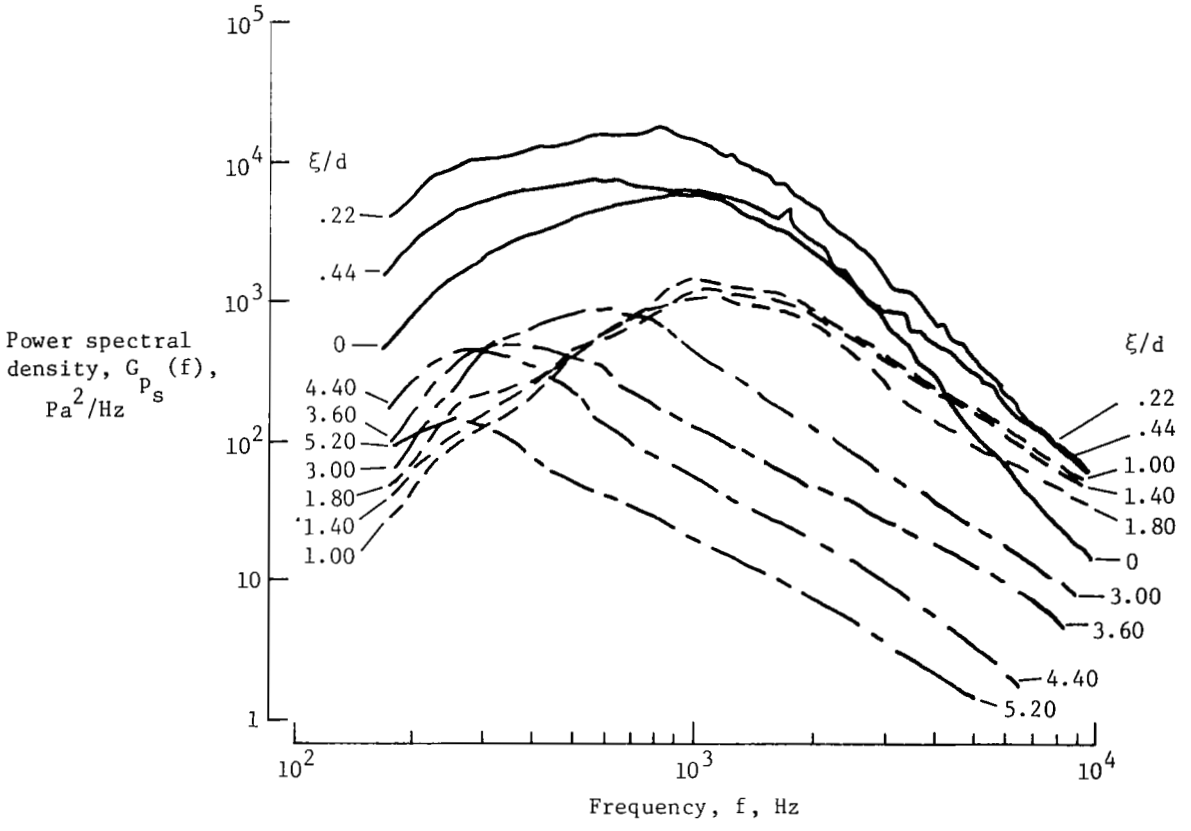

Figure 8.- Power spectral density of fluctuating surface pressure at several radial distances ξ/d. $M_j = 0.70$; $h/d = 5$.

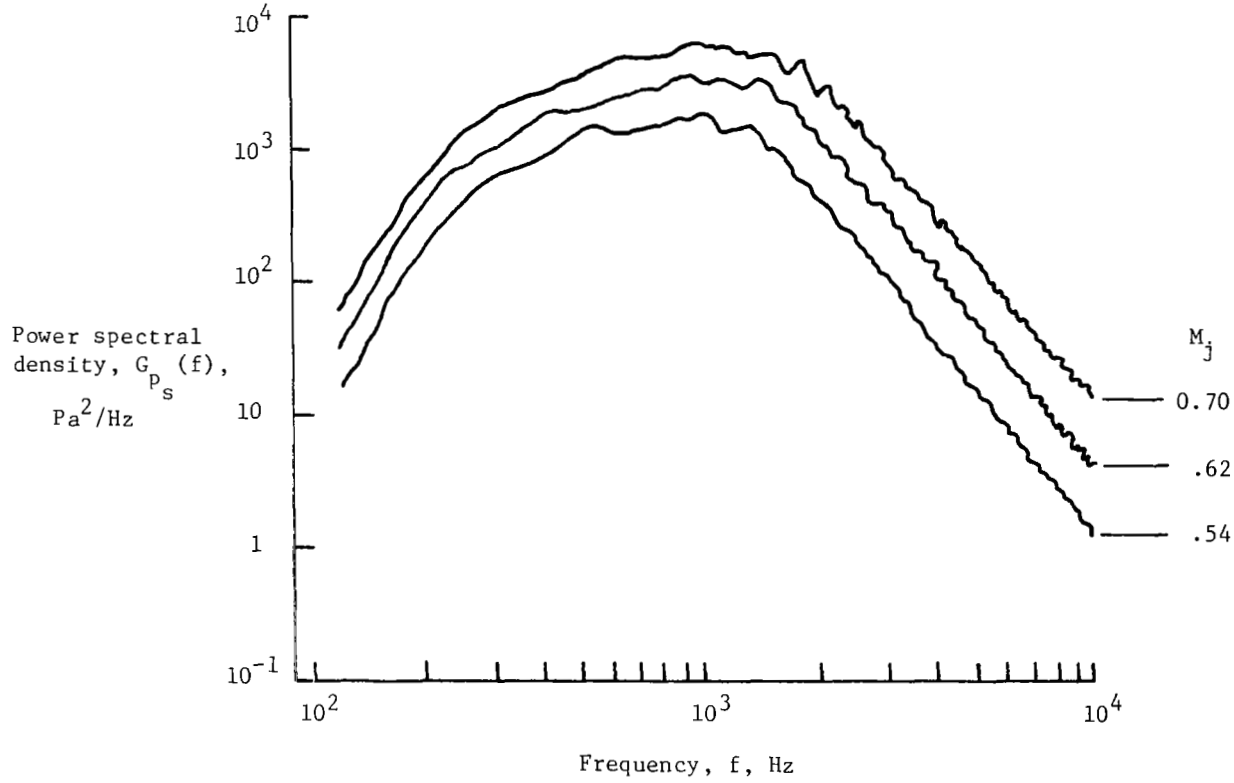

(a) $\xi/d = 0$.

Figure 9.- Power spectral density of fluctuating surface pressure at several jet Mach numbers. $h/d = 5$.

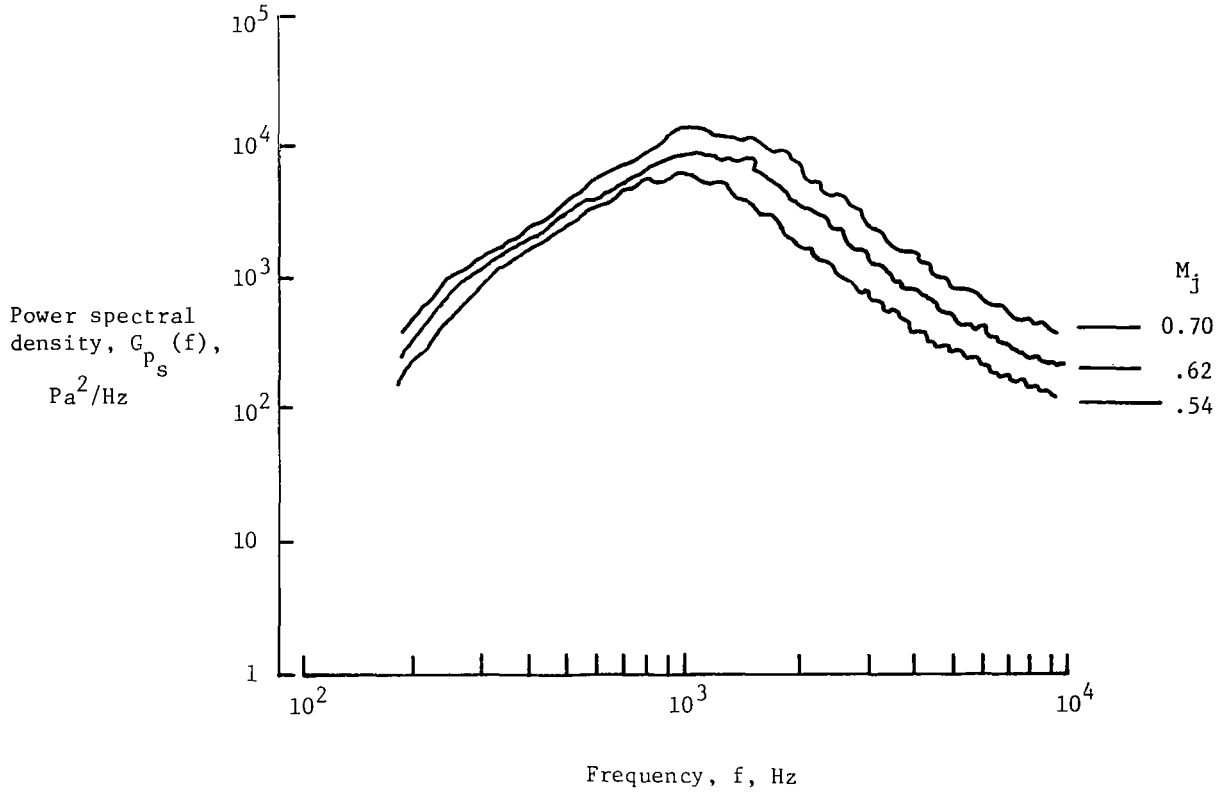

(b) $\xi/d = 1.80$.

Figure 9.- Concluded.

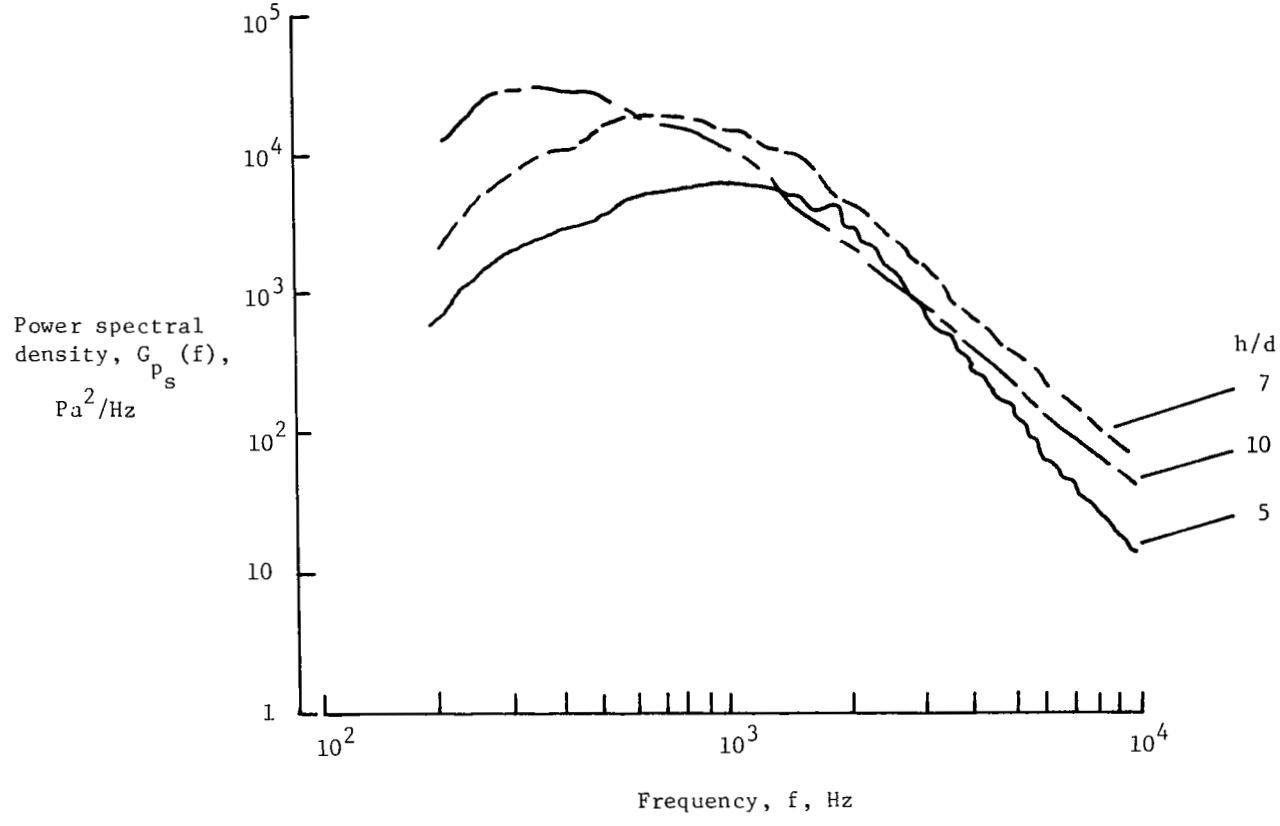

(a) $\xi/d = 0$.

Figure 10.- Power spectral density of fluctuating surface pressure at several jet heights. $M_j = 0.70$.

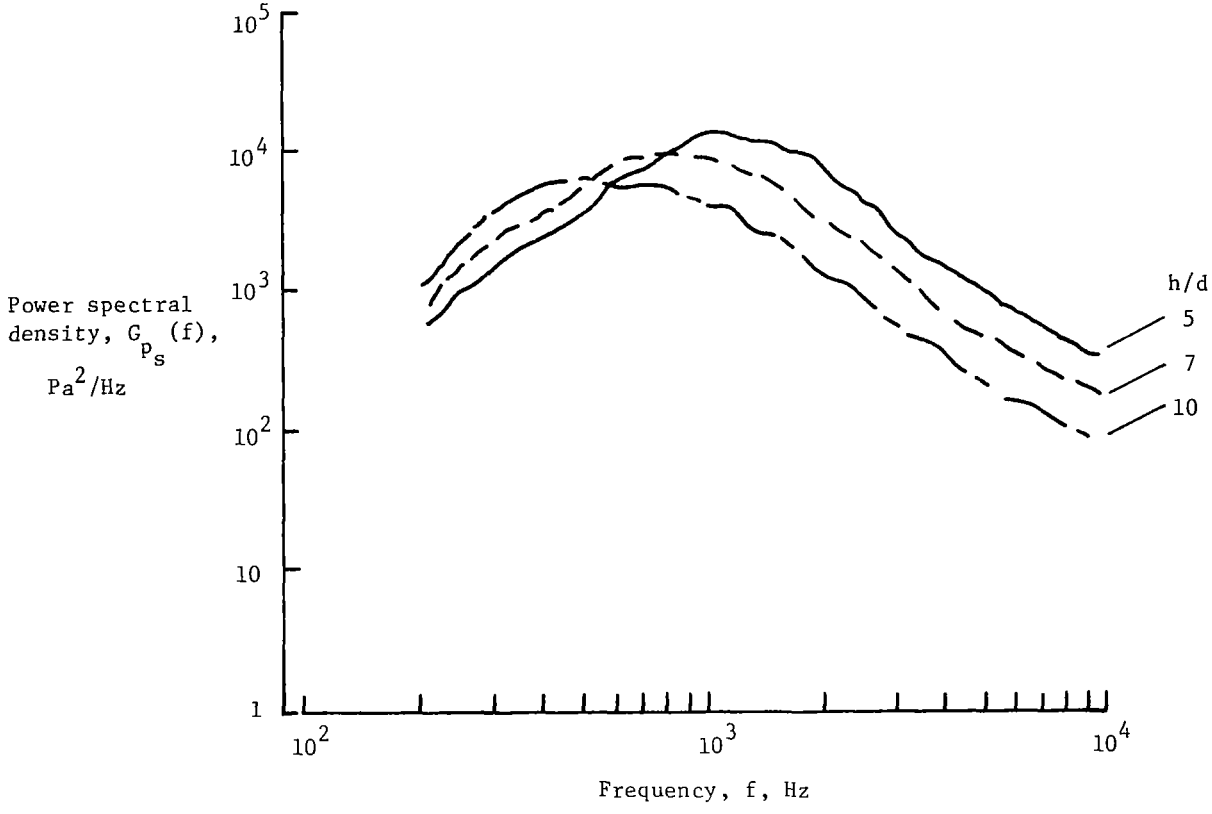

(b) $\xi/d = 1.80$.

Figure 10.- Concluded.

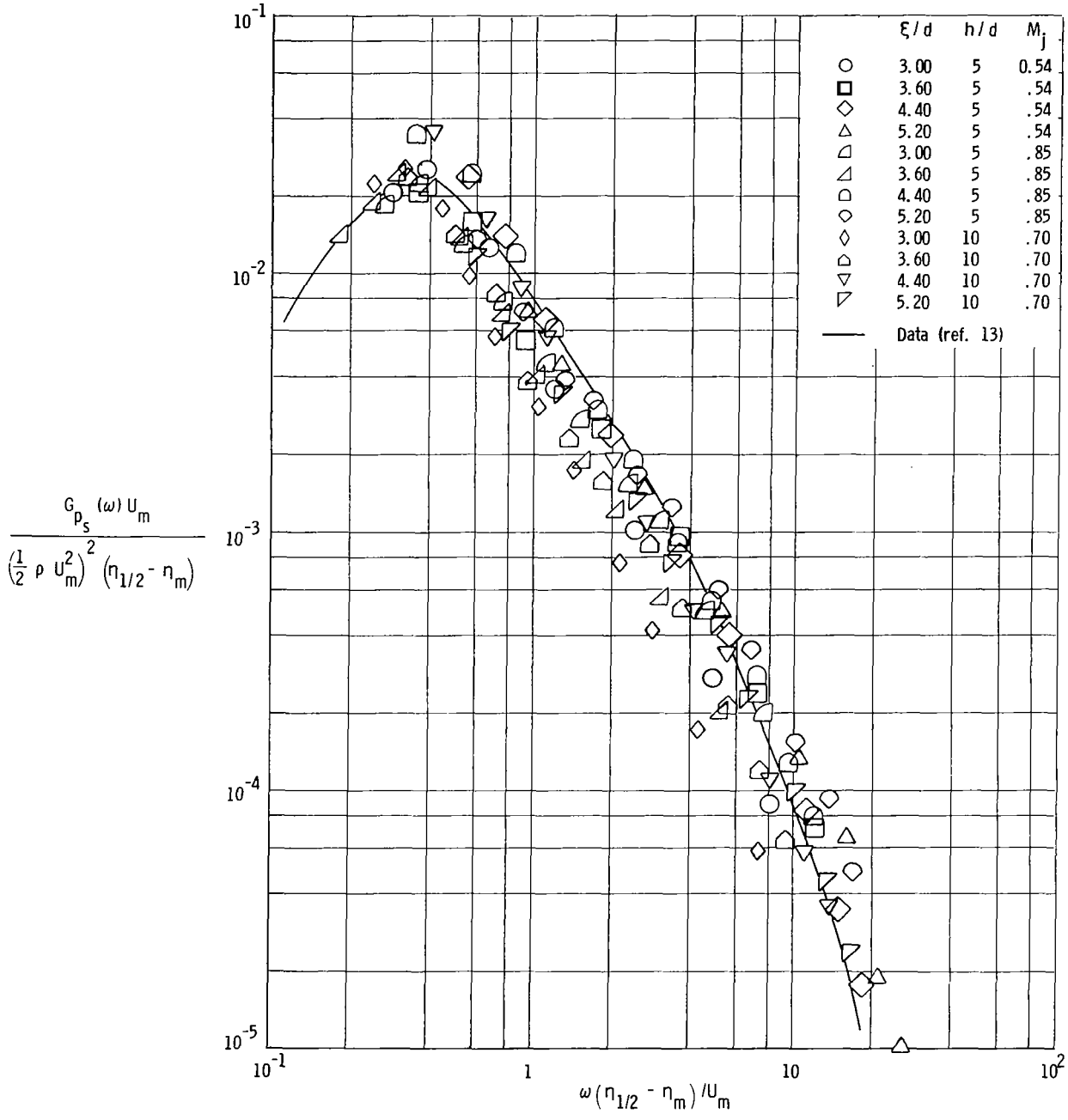

Figure 11.- Nondimensional power spectral density of fluctuating surface pressure in wall-jet regime.

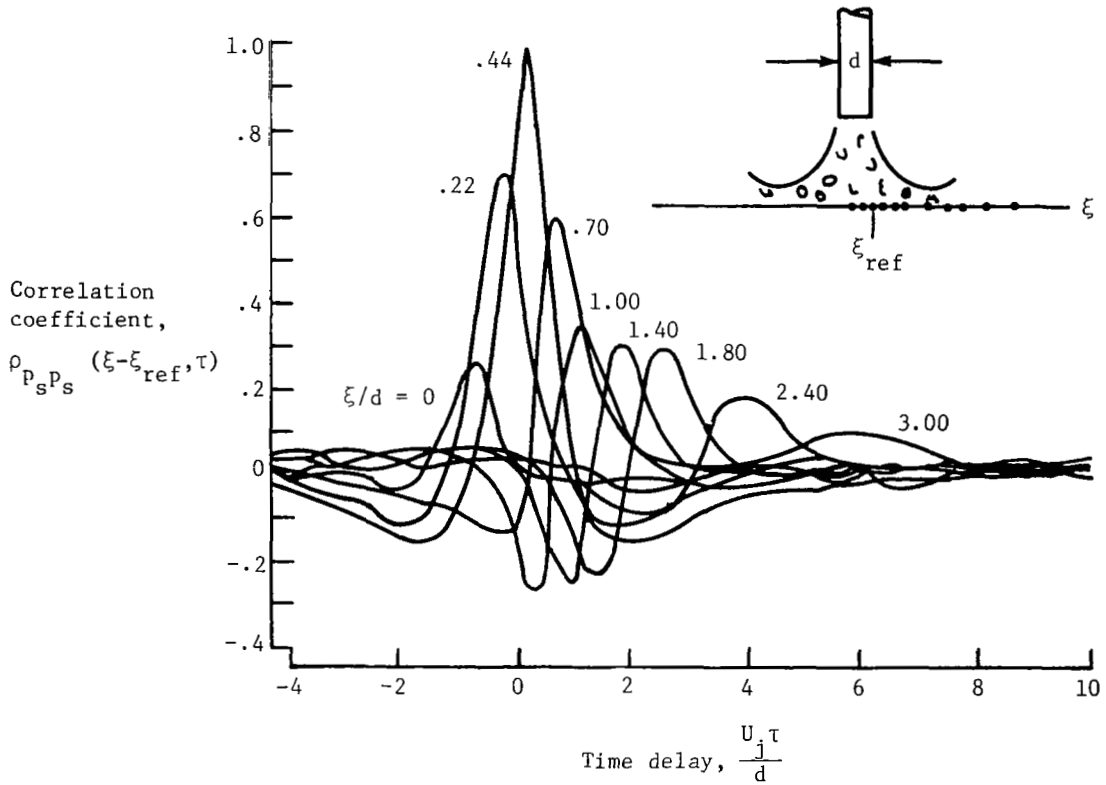

Figure 12.- Space-time correlations of fluctuating surface pressure (relative to $\xi_{ref} = 0.44d$). $M_j = 0.70$; $h/d = 5$.

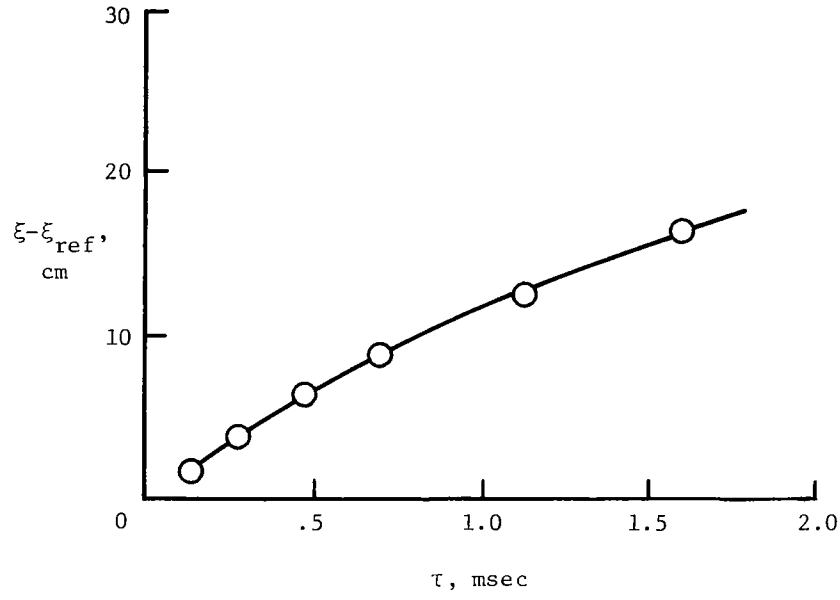

(a) Transducer separation versus time delay.

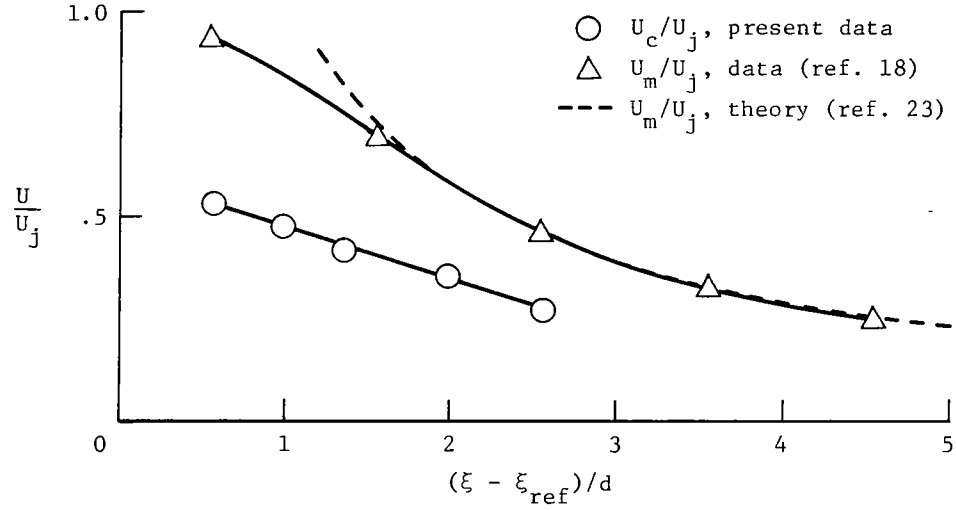

(b) Variation of eddy convection velocity with separation distance.

Figure 13.- Determination of local eddy convection velocity. $M_j = 0.70$; $h/d = 5$.

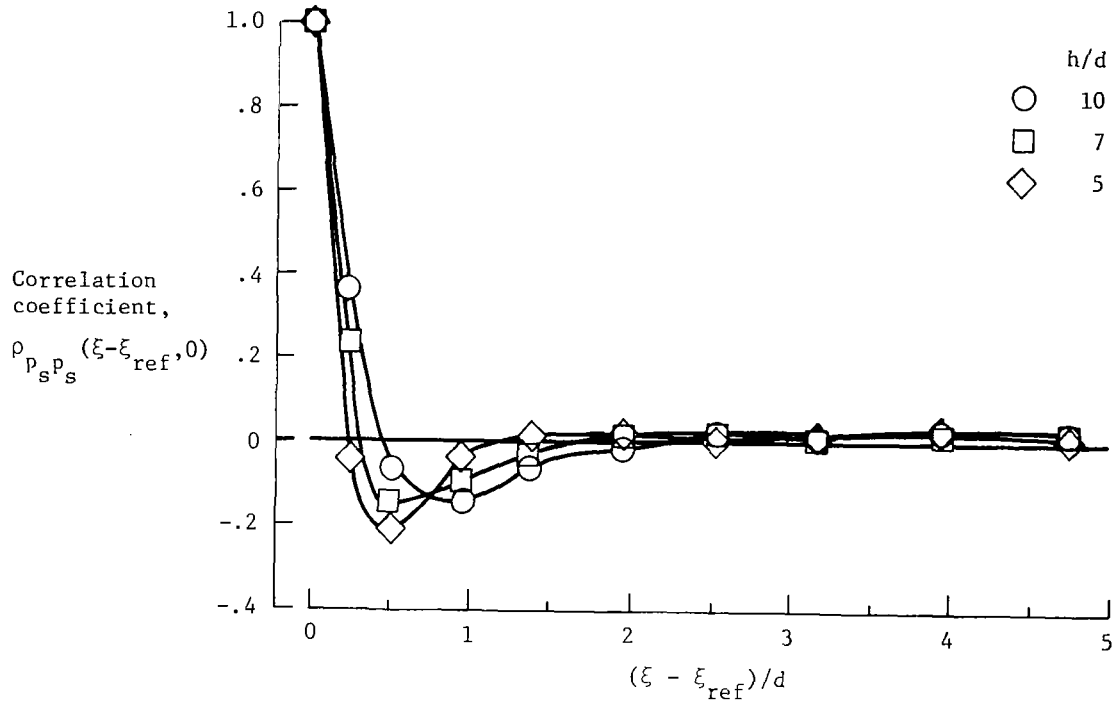

Figure 14.- Space correlations of fluctuating surface pressure for several values of h/d. $M_j = 0.70$.

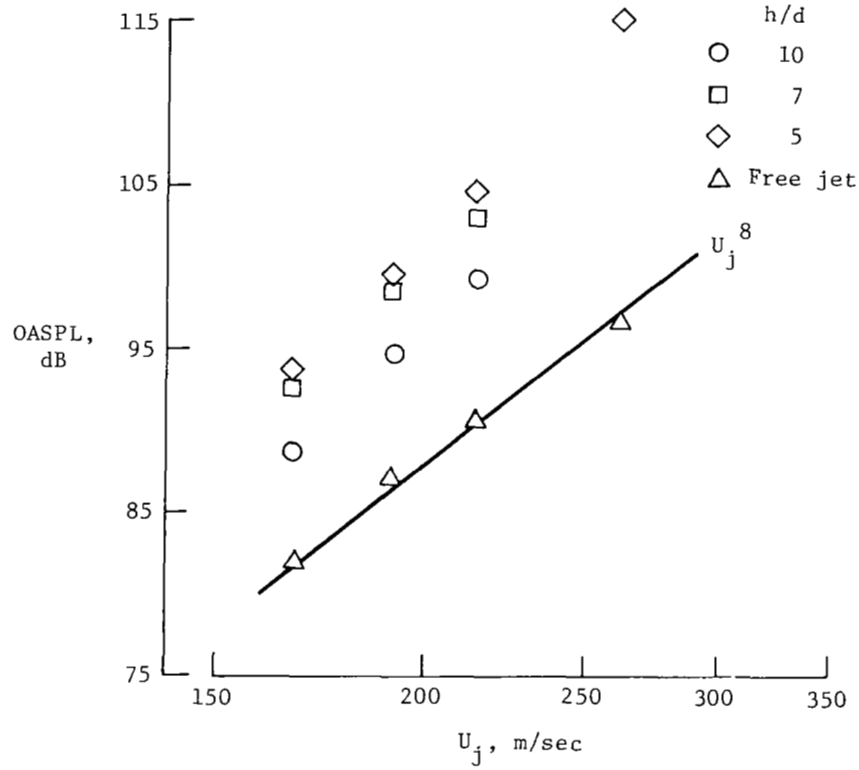

Figure 15.- Variation of overall sound pressure level with jet velocity for various jet heights and for the free jet. $\theta = 55^{o}$.

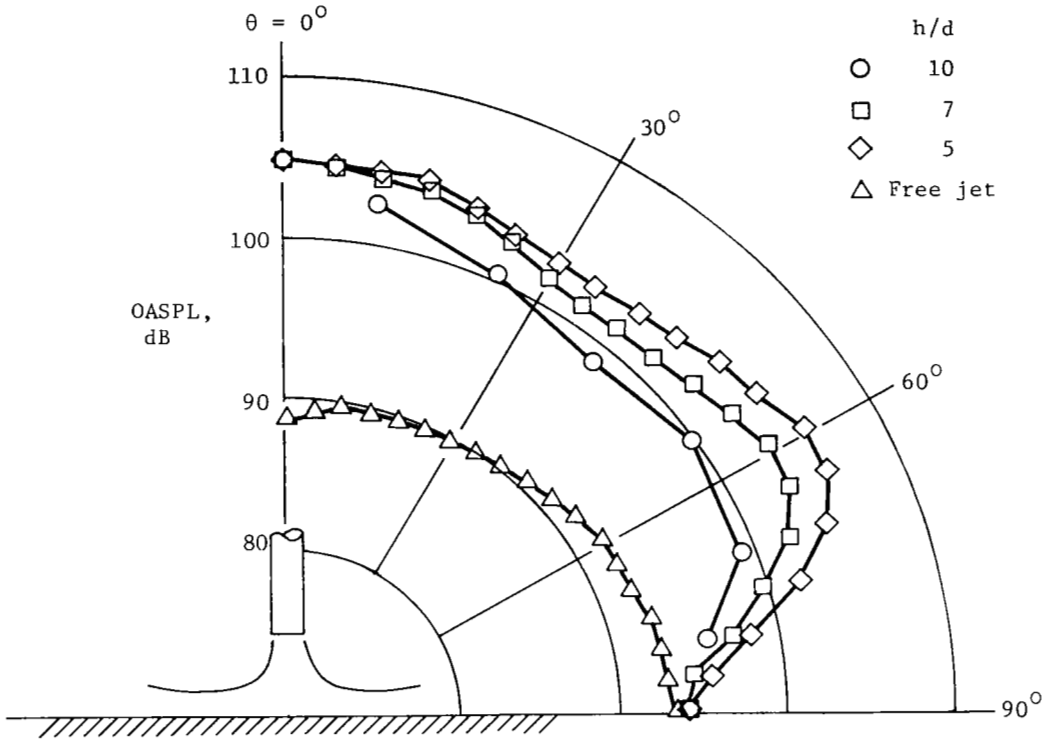

Figure 16.- Directivity patterns. $M_j = 0.70$.

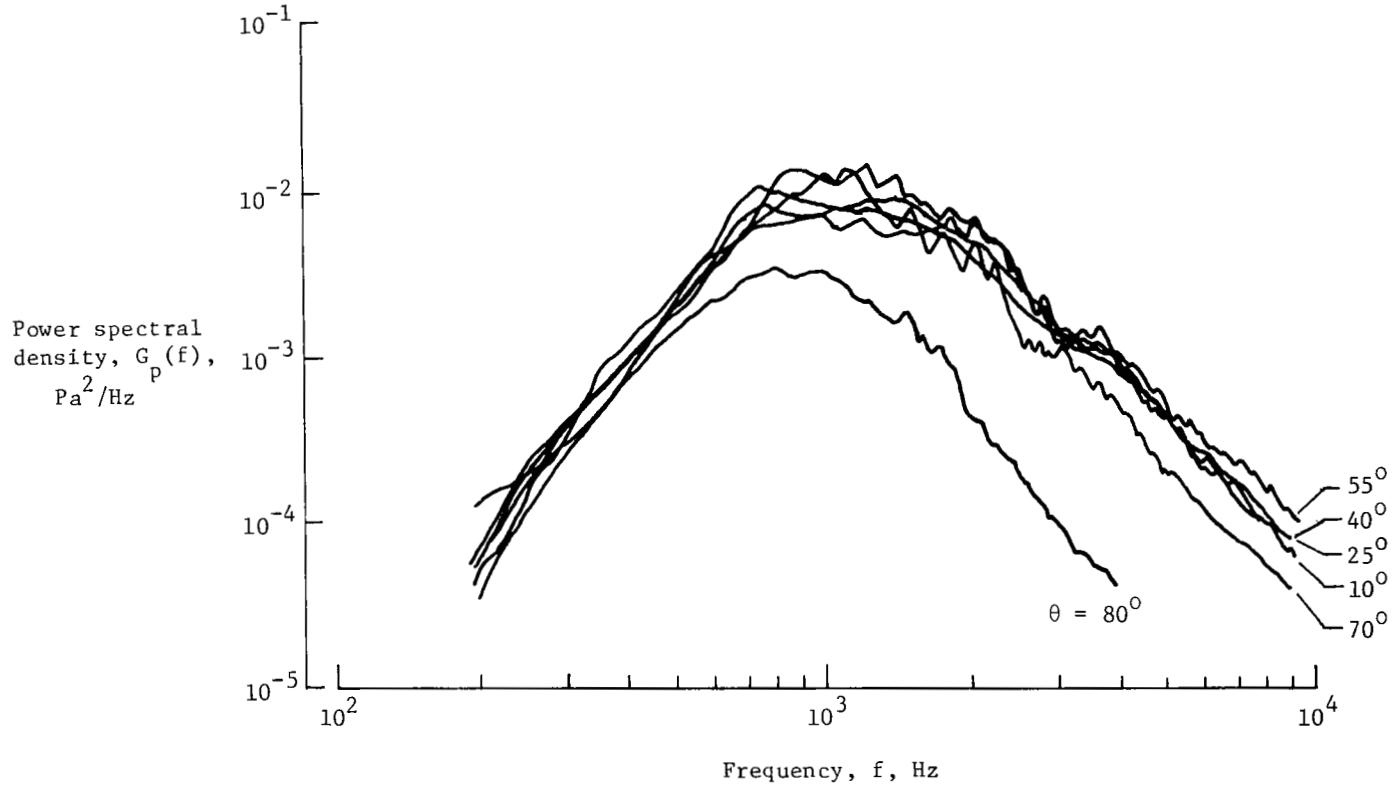

Figure 17.- Power spectral density of far-field noise at several angle positions.
$M_j = 0.70$; $h/d = 5$.

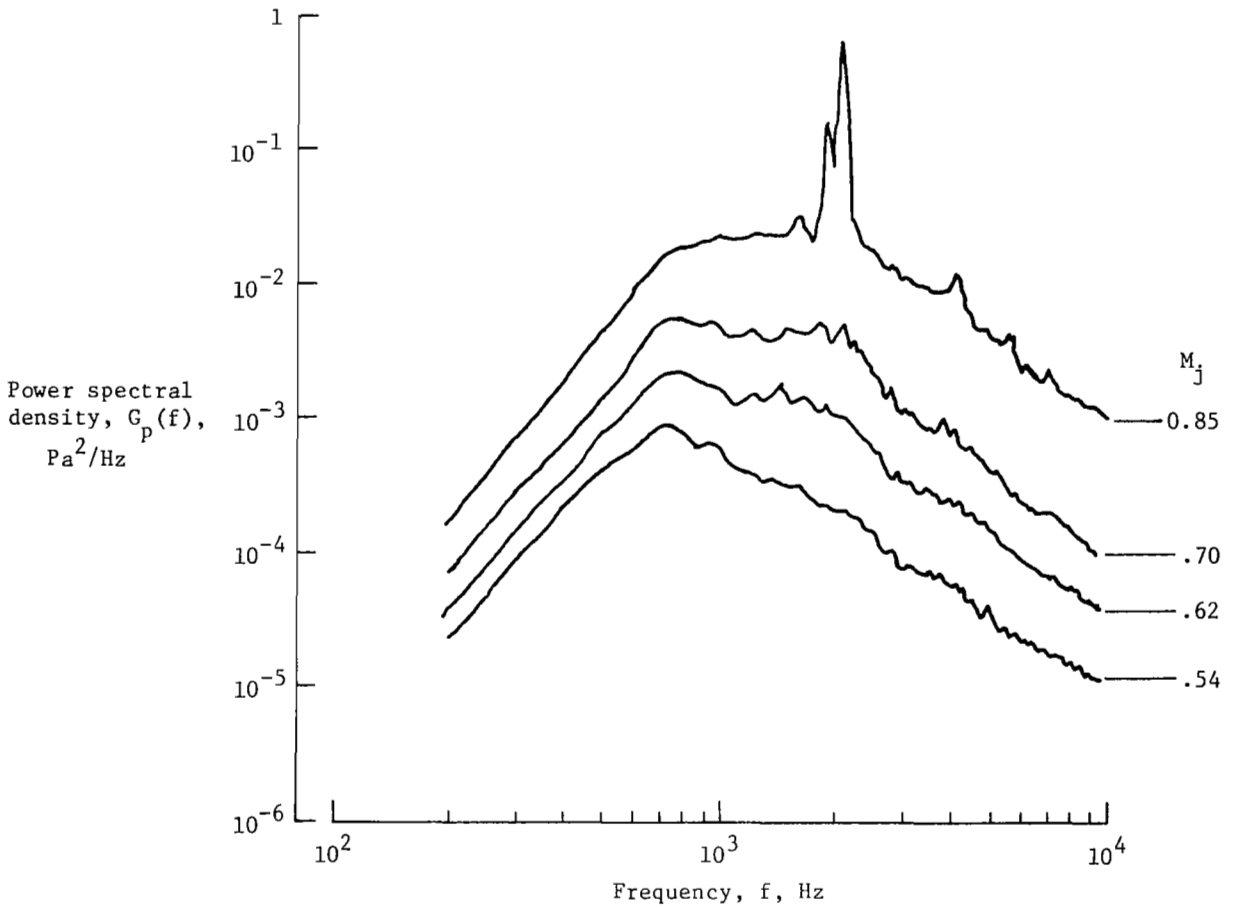

Figure 18.- Power spectral density of far-field noise at several jet Mach numbers. h/d = 5; $\theta = 55^{o}$.

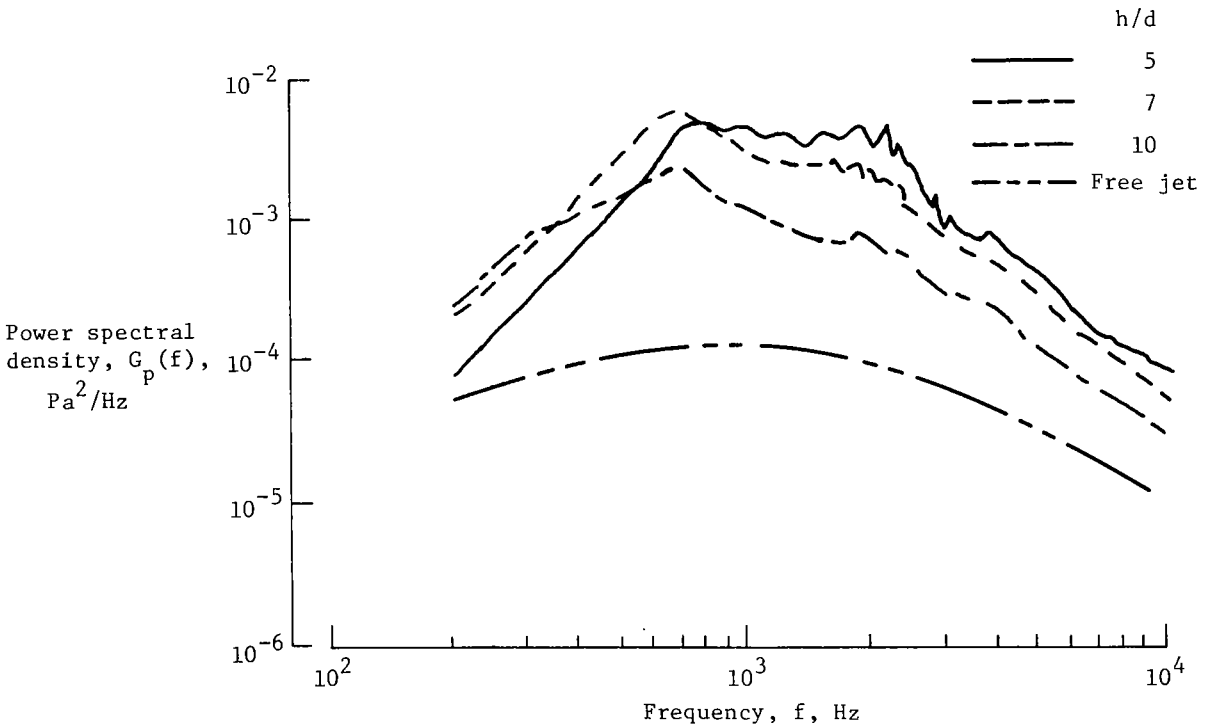

Figure 19.- Power spectral density of far-field noise at several jet heights. $M_j = 0.70$; $\theta = 55^o$.

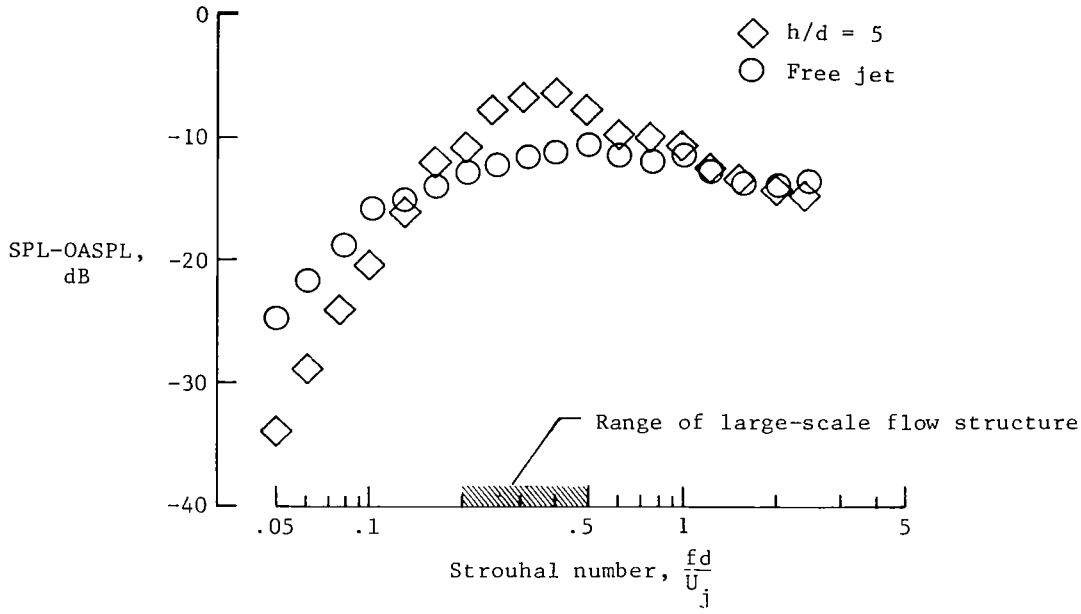

Figure 20.- Comparison of free and impinging jet noise spectra.
$h/d = 5$; $M_j = 0.70$; $\theta = 55^{o}$.

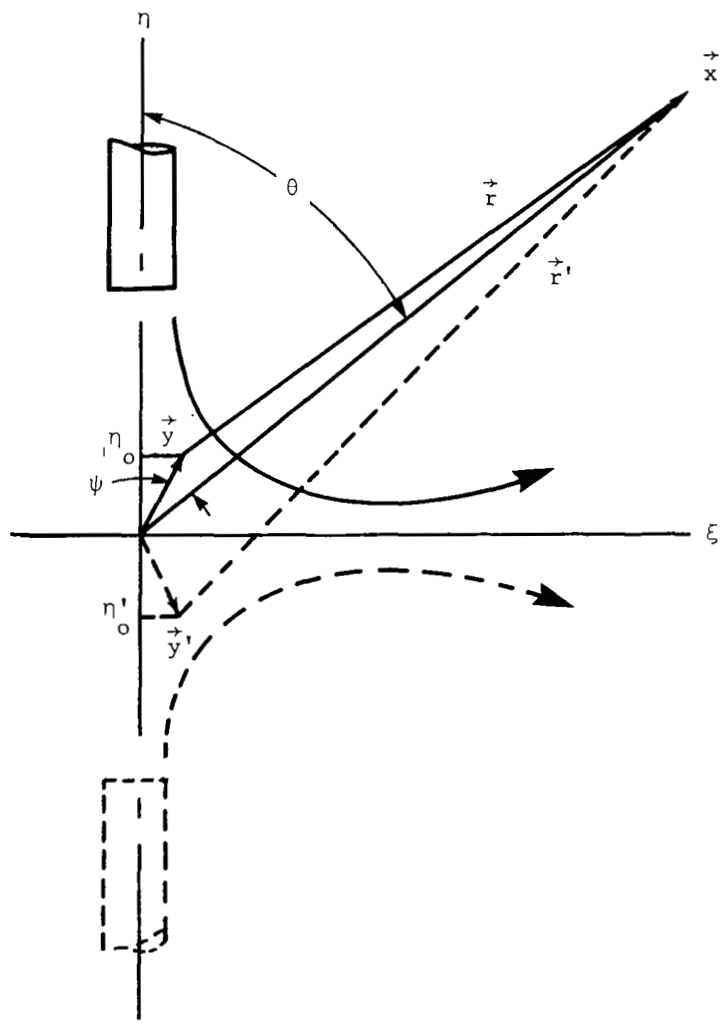

Figure 21.- Sketch of real and image flow systems with typical source and field point locations.

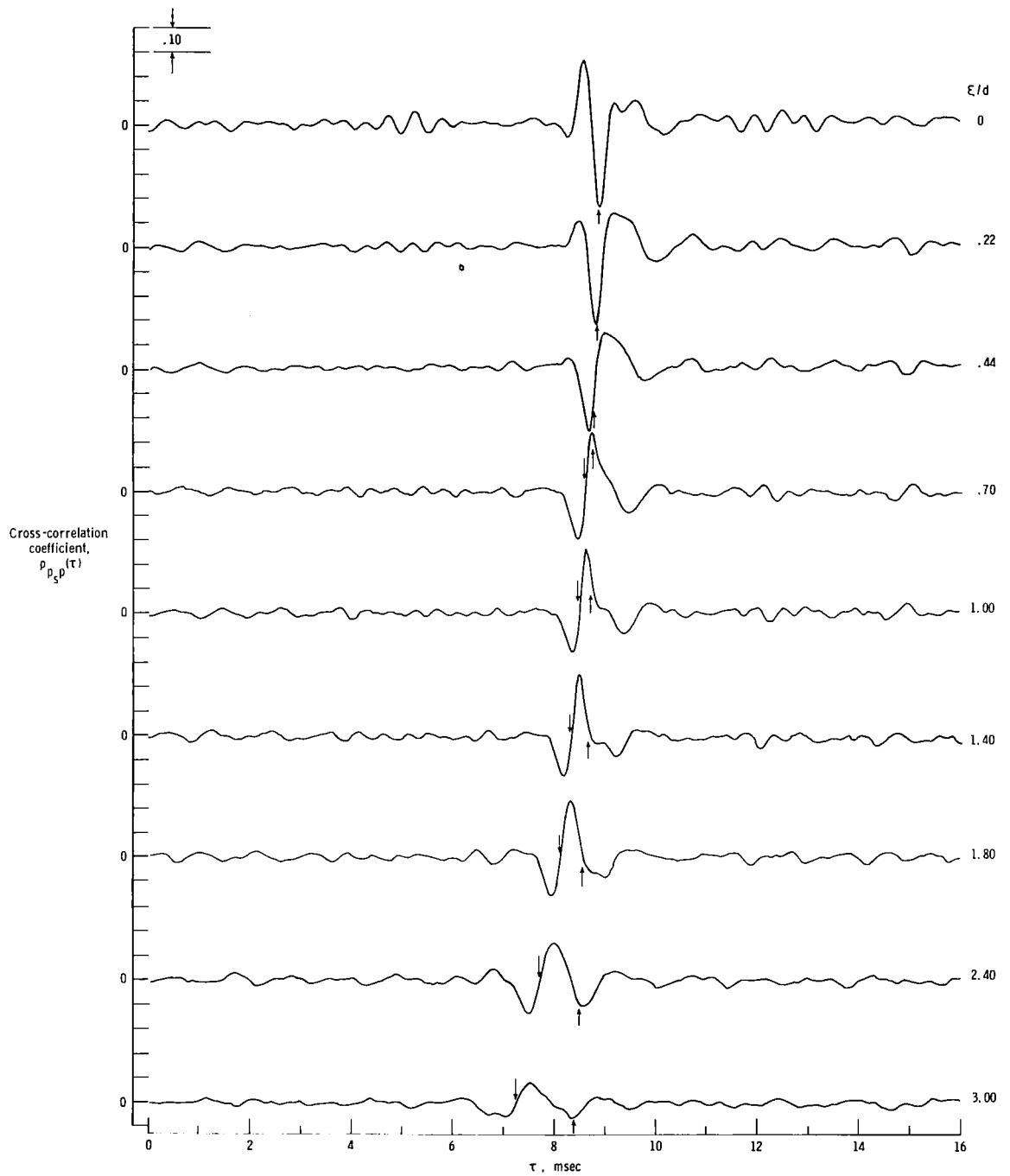

(a) $M_j = 0.70$; $\theta = 55^o$; $h/d = 5$.

Figure 22.- Cross-correlation coefficient between surface and far-field pressures. Upward-pointing arrows indicate delay time of r/c. Downward pointing arrows indicate delay time where the rate of change of the function is largest.

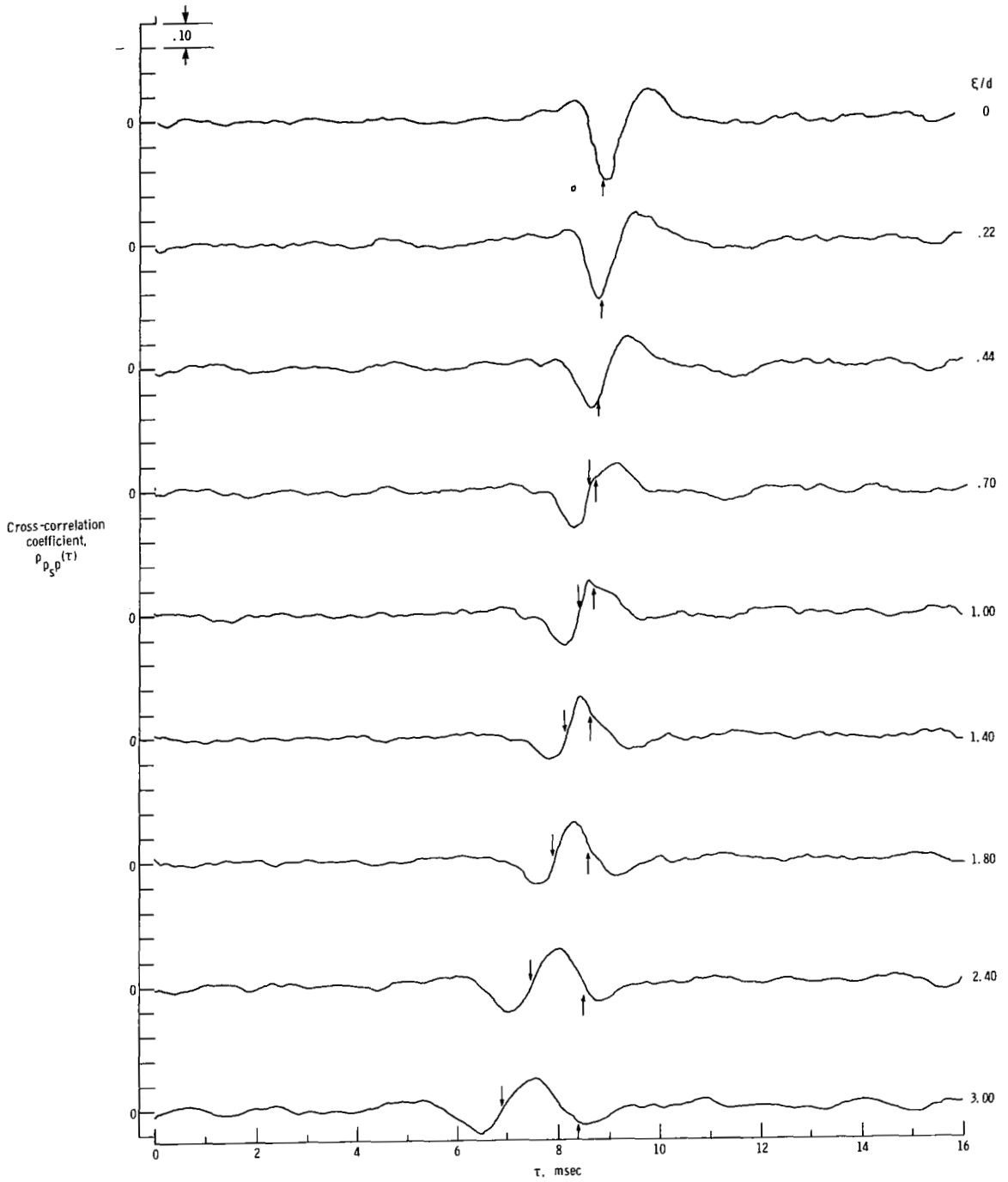

(b) $M_j = 0.70$; $\theta = 55^{\circ}$; $h/d = 10$.

Figure 22.- Concluded.

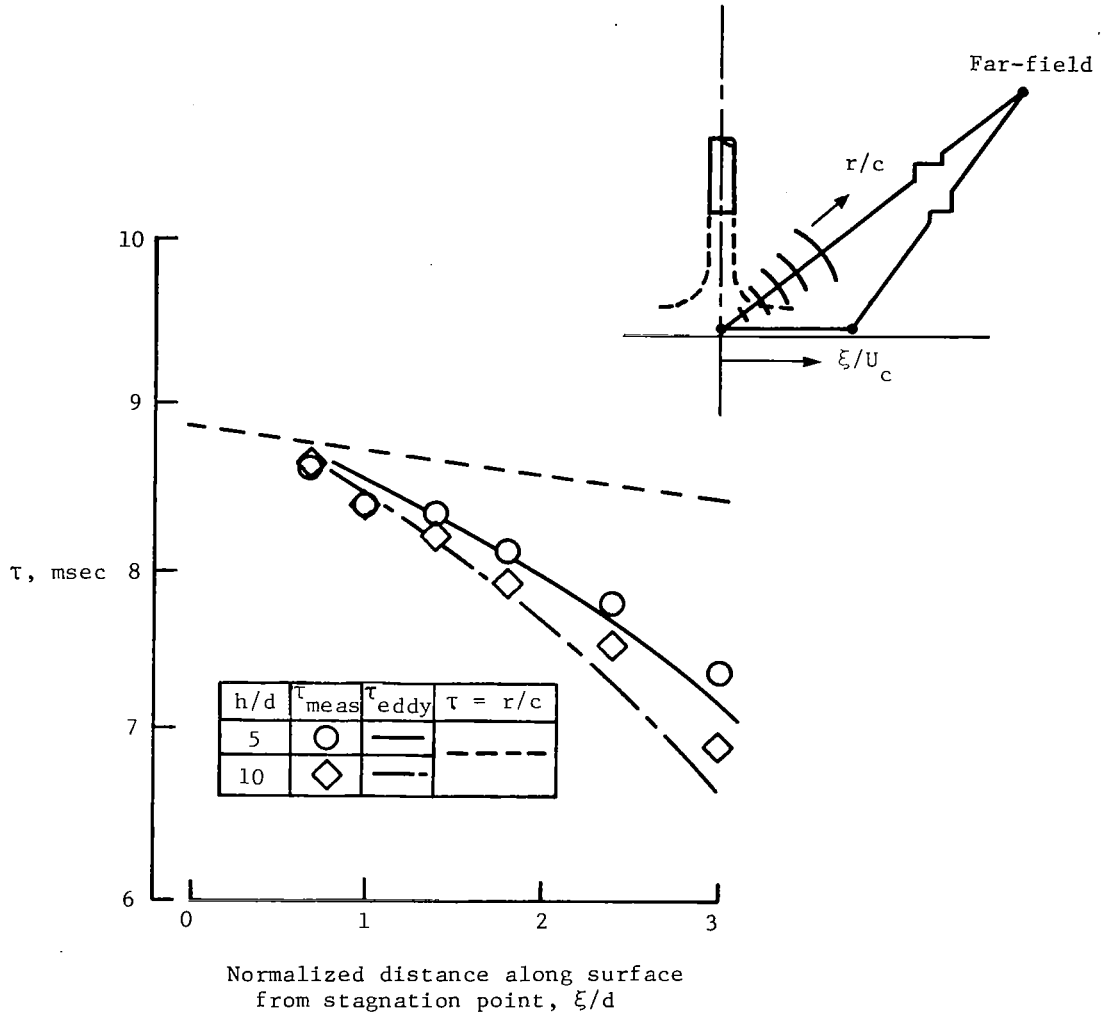

Figure 23.- Comparison between measured and calculated delay times.

1. Report No.	2. Government Accession No.	3. Recipient's Catalog No.
NASA TP-1361		

4. Title and Subtitle	5. Report Date
FLUCTUATING SURFACE PRESSURE AND ACOUSTIC RADIATION FOR SUBSONIC NORMAL JET IMPINGEMENT	March 1979
	6. Performing Organization Code
7. Author(s)	8. Performing Organization Report No.
John S. Preisser	L-12412
	10. Work Unit No.
9. Performing Organization Name and Address	505-06-23-01
NASA Langley Research Center Hampton, VA 23665	11. Contract or Grant No.
	13. Type of Report and Period Covered
12. Sponsoring Agency Name and Address	Technical Paper
National Aeronautics and Space Administration Washington, DC 20546	14. Sponsoring Agency Code

15. Supplementary Notes

16. Abstract

This report presents results from an experimental study of fluctuating surface pressures and far-field noise produced by a subsonic circular jet impinging normally to a large, rigid, flat surface. The tests were performed in an anechoic room for jet Mach numbers from 0.54 to 0.85 and for jet-to-surface heights from 5 to 10 jet diameters. Space and time correlations of surface pressure indicated a radially spreading, decaying pressure field having correlation lengths on the order of one-half the jet diameter with convection speeds between 0.5 and 0.6 of the peak wall-jet velocity. Overall sound pressure level varied as the eighth power of the jet velocity. Large-scale orderly structures in the flow were suggested by the noise spectra which peaked at a Strouhal number of about 0.3. In addition, an analytical formulation was given to approximate the apparent noise-producing regions of the flow in terms of cross-correlations and cross-spectra between the surface and far-field measurements. Results pointed to the impingement region of the flow field as the major contributor to the far-field impingement noise.

17. Key Words (Suggested by Author(s))	18. Distribution Statement
Jet impingement Fluctuating surface pressure Flow-surface interaction noise	Unclassified – Unlimited Subject Category 71

19. Security Classif. (of this report)	20. Security Classif. (of this page)	21. No. of Pages	22. Price*
Unclassified	Unclassified	53	$5.25

*For sale by the National Technical Information Service, Springfield, Virginia 22161

NASA-Langley, 1979

4 1 1U,H, 021779 S00903DS
DEPT OF THE AIR FORCE
AF WEAPONS LABORATORY
ATTN: TECHNICAL LIBRARY (SUL)
KIRTLAND AFB NM 87117